Circulation Research

ORIGINAL RESEARCH

Reversal of Pulmonary Hypertension in a Human-Like Model: Therapeutic Targeting of Endothelial DHFR

Priya Murugesan,* Yixuan Zhang,* Yuanli Huang,* Nobel Chenggong Zong,* Ji Youn Youn, Wenhui Chen, Chen Wang, Joseph Loscalzo, Hua Cai

BACKGROUND: Pulmonary hypertension (PH) is a progressive disorder characterized by remodeling of the pulmonary vasculature and elevated mean pulmonary arterial pressure, resulting in right heart failure.

METHODS: Here, we show that direct targeting of the endothelium to uncouple eNOS (endothelial nitric oxide synthase) with DAHP (2,4-diamino 6-hydroxypyrimidine; an inhibitor of GTP cyclohydrolase 1, the rate-limiting synthetic enzyme for the critical eNOS cofactor tetrahydrobiopterin) induces human-like, time-dependent progression of PH phenotypes in mice.

RESULTS: Critical phenotypic features include progressive elevation in mean pulmonary arterial pressure, right ventricular systolic blood pressure, and right ventricle (RV)/left ventricle plus septum (LV+S) weight ratio; extensive vascular remodeling of pulmonary arterioles with increased medial thickness/perivascular collagen deposition and increased expression of PCNA (proliferative cell nuclear antigen) and alpha-actin; markedly increased total and mitochondrial superoxide production, substantially reduced tetrahydrobiopterin and nitric oxide bioavailabilities; and formation of an array of human-like vascular lesions. Intriguingly, novel in-house generated endothelial-specific dihydrofolate reductase (DHFR) transgenic mice (tg-EC-DHFR) were completely protected from the pathophysiological and molecular features of PH upon DAHP treatment or hypoxia exposure. Furthermore, DHFR overexpression with a pCMV-DHFR plasmid transfection in mice after initiation of DAHP treatment completely reversed PH phenotypes. DHFR knockout mice spontaneously developed PH at baseline and had no additional deterioration in response to hypoxia, indicating an intrinsic role of DHFR deficiency in causing PH. RNA-sequencing experiments indicated great similarity in gene regulation profiles between the DAHP model and human patients with PH.

CONCLUSIONS: Taken together, these results establish a novel human-like murine model of PH that has long been lacking in the field, which can be broadly used for future mechanistic and translational studies. These data also indicate that targeting endothelial DHFR deficiency represents a novel and robust therapeutic strategy for the treatment of PH.

GRAPHIC ABSTRACT: A graphic abstract is available for this article.

Key Words: hypertension ■ hypoxia ■ mitochondria ■ nitric oxide synthase type III ■ oxidative stress ■ pulmonary ■ therapeutics ■ vascular remodeling

In This Issue, see p 343 | Meet the First Author, see p 344

Pulmonary hypertension (PH) is a severe cardiopulmonary disorder characterized by the remodeling of the small pulmonary blood vessels, resulting in a progressive increase in pulmonary vascular resistance, right ventricular (RV) hypertrophy, and ultimately right heart failure.[1,2] Endothelial cells (ECs) and nitric oxide

Correspondence to: Hua Cai, MD, PhD, Division of Molecular Medicine, Department of Anesthesiology, Division of Cardiology, Department of Medicine, David Geffen School of Medicine, University of California, Los Angeles, CA, 90095, Email hcai@mednet.ucla.edu; or Joseph Loscalzo, MD, PhD, Department of Medicine, Brigham and Women's Hospital, Harvard Medical School, Boston, MA, 02115, Email jloscalzo@rics. bwh.harvard.edu; or Chen Wang, MD, PhD, Peking Union Medical College and Chinese Academy of Medical Sciences, 100005, Beijing, China, wangchen66366@163.com
*P. Murugesan, Y. Zhang, Y. Huang, and NC Zong contributed equally.
Supplemental Material is available at https://www.ahajournals.org/doi/suppl/10.1161/CIRCRESAHA.123.323090.
For Sources of Funding and Disclosures, see page 369.

Circulation Research is available at www.ahajournals.org/journal/res

ORIGINAL RESEARCH

Novelty and Significance

What Is Known?

- Pulmonary hypertension (PH) is a severe and devastating cardiorespiratory disease with limited therapeutic options leading to regression.
- Current clinical strategies improve symptoms of the disease but do not halt progression.
- No human-like preclinical model is available to enable rapid translational studies.

What New Information Does This Article Contribute?

- Our studies establish a human-like murine model of PH with phenotypic and genetic features simulating human PH, enabling in-depth mechanistic and translational studies of PH.
- Our findings demonstrate a critical intermediate role for endothelial dihydrofolate reductase (DHFR) deficiency in the development of PH. DAHP (2,4-diamino 6-hydroxypyrimidine) or hypoxia exposure induced PH in mice, which was completely prevented in endothelial DHFR transgenic mice (tg-EC-DHFR). DHFR knockout mice displayed spontaneous PH that was not affected by additional hypoxia exposure.
- Our findings demonstrate that gene therapy with DHFR after initiation of PH completely reversed progress of PH.
- These studies show that targeting endothelial DHFR deficiency may represent a novel and robust therapeutic strategy for the treatment of PH.

PH is a severe and devastating cardiorespiratory disease. Limited human-like preclinical models are available for mechanistic and translational studies. In the present study, we for the first time established a murine model of PH that is human-like in both phenotypic and molecular features, enabling in-depth studies of PH. Our findings also demonstrate a critical intermediate role of endothelial DHFR deficiency in the development of PH, which can be targeted to effectively treat and regress PH.

Nonstandard Abbreviations and Acronyms

BMPR2	bone morphogenetic protein receptor type 2
DAHP	2,4-diamino 6-hydroxypyrimidine
DEG	differentially expressed gene
DHFR	dihydrofolate reductase
EC	endothelial cell
eNOS	endothelial nitric oxide synthase
ET-1	endothelin-1
GTPCHI	GTP cyclohydrolase 1
IL-6	interleukin-6
mPAP	mean pulmonary arterial pressure
NO	nitric oxide
PCNA	proliferative cell nuclear antigen
PDE5	phosphodiesterase 5
PH	pulmonary hypertension
RV	right ventricular
RVSP	right ventricular systolic blood pressure
SMA	smooth muscle α-actin
WT	wild-type

(NO) derived from the pulmonary endothelium[3] are recognized as major regulators of vascular function in the pulmonary circulation, while endothelial dysfunction is involved in the imbalanced production of vasoconstrictors and vasodilators and of activators and inhibitors of smooth muscle cell growth and migration,[4] as well as in the generation of a prothrombotic vascular (micro)environment.[5] Endothelial dysfunction has been implicated as a primary cause of idiopathic PH,[6] and hyperproliferative ECs contribute to advanced lesion formation.[7] Therapies targeting the NO-cGMP signaling pathway have been used as pulmonary vasodilators and antithrombotic agents to improve vascular perfusion, hemodynamics, functional status, and symptoms in patients with PH. These include inhaled NO, PDE5 (phosphodiesterase 5) inhibitors (sildenafil and tadalafil), and cGMP agonists (riociguat).[8–11] The other two classes of drugs target ET-1 (endothelin-1) and prostacyclin to improve vascular function. None of these treatments, however, targets vascular remodeling, the later stage of the disease, which is necessary to mitigate the more profound consequences of the disease and effectively stop or regress PH. None of these treatments has the advantageous effects of targeting dihydrofolate reductase (DHFR), as we show in the present study, to alleviate oxidative stress at the same time of improving NO-mediated vasodilation and protecting against vascular remodeling.

One of the major limitations of mechanistic and therapeutic studies of PH is the lack of a preclinical or human-like animal model of PH that replicates the human disease.[12] Of note, monocrotaline and chronic hypoxia are two well-studied and widely used animal models of PH. These models are considered to recapitulate the first phase of the disease and, therefore, used for development of drugs targeting vasoconstriction rather than those that target the progressive remodeling phase of PH. Additional animal models include combinations of several

interventions, such as exposure to monocrotaline with left pneumonectomy or injection of Sugen (SU5416) followed by hypoxia. Other potential approaches are based on genetic manipulation, for example, overexpression of calcium-binding protein (S100A4/Mts1) or IL-6 (interleukin-6), or deletion of BMPR2 (bone morphogenetic protein receptor type 2).[13,14] Despite their widespread use, the experimental PH community recognizes that these animal models do not recapitulate human disease with adequate fidelity. The monocrotaline model offers advantages in highlighting the contributions of pulmonary artery injury characterized by endothelial damage, in situ thrombosis, perivascular inflammation, fibrosis, and the development of pulmonary edema.[15,16] Plexiform lesions are seen if monocrotaline is administered to pneumonectomized rats or in combination with chronic hypoxia.[16] However, monocrotaline may exert direct toxicity on the heart or other organs via endothelial toxicity, making it difficult to isolate the effects of pressure overload from other direct toxic effects on the right ventricle. In addition, the plasma cytokine profile of monocrotaline-induced PH in rodents does not match well with that of human pulmonary arterial hypertension (PAH).[16] The SU5416-hypoxia mouse model displays severe pulmonary vascular remodeling even in the absence of chronic hypoxia.[17] However, the degree of vascular remodeling in mice is not the same as in human disease, lacking neointima formation.[18] In addition, the PH phenotype is reversed upon return to normoxia,[19] and severe RV failure is not a feature of the model.[20] Hence, to facilitate molecular mechanistic and translational studies of PH, it is critical to establish novel human-like animal models of the disease.

Accumulating evidence has demonstrated that eNOS (endothelial nitric oxide synthase) cofactor tetrahydrobiopterin (H_4B) plays a critical role in determining eNOS coupling/uncoupling activity. When tetrahydrobiopterin bioavailability is low consequent to oxidative inactivation and a deficiency in its salvage enzyme DHFR, electrons are diverted to molecular oxygen rather than to L-arginine, transforming eNOS into a superoxide anion-generating pro-oxidant enzyme, denoted as uncoupled eNOS.[21–41] This transformation of eNOS has been observed in several in vitro models, animal models, and human patients with cardiovascular diseases, including hypertension, aortic aneurysms, atherosclerosis, diabetic vascular complications, cardiac ischemia reperfusion injury, and heart failure.[21–41] In view of the critical role of endothelial dysfunction in initiating the pathophysiological processes of PH, we hypothesize that uncoupling of eNOS might have a direct causal role in the development of PH, which might be used to establish an animal model that resembles human PH or idiopathic PH.

Administration of DAHP (2,4-diamino 6-hydroxypyrimidine) into mice to uncouple eNOS directly via inhibition of GTP cyclohydrolase 1 (GTPCHI, rate-limiting synthetic enzyme for tetrahydrobiopterin) resulted in progressively and markedly elevated mean pulmonary arterial pressure (mPAP) and RV systolic blood pressure (RVSP), and increased expression of proliferative cell nuclear antigen (PCNA) and alpha-actin in pulmonary blood vessels; extensive vascular remodeling characterized by a full spectrum of human PH-like lesions of medial thickening, intimal thickness, plexiform lesions, aneurysm-like lesions, anarchous growth of cells that completely obliterate the vascular lumen, bud-like lesions covered by an endothelial layer, and disorganized stalk-like lesions comprising hyperchromatic and oval cells inside the lumen of pulmonary arteries and recanalized lesions; and accompanying features of reduced tetrahydrobiopterin and NO bioavailabilities, increased eNOS uncoupling activity, and increased total and mitochondrial superoxide production. Importantly, we have generated a novel strain of mice that overexpress DHFR specifically in ECs, endothelial specific DHFR transgenic mice (tg-EC-DHFR), and found that these animals were remarkably protected from PH development in response to both DAHP administration or hypoxia exposure, with all of the pathophysiological and molecular features fully attenuated, indicating a robust therapeutic effect on PH of targeting the DHFR-eNOS axis. Importantly, DHFR overexpression with pCMV-DHFR plasmid transfection in mice after initiation of DAHP administration completely reversed PH phenotypes, further confirming a robust therapeutic effect of DHFR overexpression on regression of PH.

Of note, DHFR knockout mice displayed elevated mPAP and RVSP, with all of the pathophysiological and molecular features of PH simulating DAHP-treated mice. Hypoxia exposure to DHFR knockout mice showed no significant additional impact, indicating an intrinsic role of DHFR deficiency in triggering the development of PH. To further examine the potential similarity between the DAHP model and human PH, we compared gene regulation profile in lung samples of human patients with PH collected during transplantation, to those of mice given DAHP treatment or hypoxia exposure. The data indicate that comparing to the hypoxia model, the gene regulation profile in the novel DAHP-induced PH model is much more similar to that of human patients with PH. Taken together, these data demonstrate that targeting endothelial DHFR represents a novel and robust therapeutic strategy for the treatment of PH.

METHODS

Data Availability

The data that support the findings of this study are available from the corresponding author upon reasonable request. For all the expanded Materials and Methods, see Supplemental Material.

RESULTS

DAHP Administration Induces Robust, Dose-Dependent Increases in mPAP and RVSP, and RV Hypertrophy

We hypothesized that DAHP inhibition GTPCHI triggers eNOS uncoupling and is directly causal of PH. DAHP is a selective inhibitor of GTPCHI, which has been documented to inhibit GTPCHI specifically resulting in reduced tetrahydrobiopterin bioavailability.[42] There has been some evidence that PH is accompanied by eNOS dysfunction and restoration of eNOS function is beneficial[43,44]; however, a direct causal role of eNOS uncoupling in the development of PH has not been established or fully characterized. Therefore, we hypothesized that DAHP administration may create a novel murine model for PH that simulates human disease via direct targeting of the endothelium, which is known to be dysfunctional in idiopathic PH.[45,46] Indeed, data indicate that DAHP-induced PH has a more similar profile of gene regulation compared with human disease than the hypoxia model of PH (see RNA-sequencing data below); and that DAHP-treated mice develop classical features of hemodynamic dysfunction (Figure 1) and a full spectrum of typical vascular lesions as seen in human patients (Figure 2).

To fully characterize the PH phenotypes in DAHP-treated mice, we first examined impact on hemodynamic parameters of DAHP administration in mice. As shown in Figure 1A, mPAP was substantially increased in mice treated with 10-mmol/L DAHP for 3 weeks (18.95±0.96 versus 36.45±3.86 mm Hg for control versus DAHP; P=0.003), 6 weeks (18.95±0.96 versus 43.11±1.20 mm Hg for control versus DAHP; P=0.002), and 9 weeks (18.95±0.96 versus 41.80±1.75 mm Hg for control versus DAHP; P=0.004). These data indicate a time-dependent response to DAHP administration in terms of mPAP elevation from 3 to 9 weeks. Moreover, data presented in Figure 1B indicate that RVSP was also substantially increased in mice treated with 10-mmol/L DAHP for 3 weeks (26.79±2.74 versus 40.83±0.98 mm Hg for control versus DAHP; P=0.0044), 6 weeks (26.79±2.74 versus 43.90±2.28 mm Hg control versus DAHP; P=0.0100), and 9 weeks (26.79±2.74 versus 52.08±2.01 mm Hg control versus DAHP; P=0.0009). The changes in RVSP were also time-dependent. Furthermore, DAHP induced RV hypertrophy as evidenced by an increased RV/(LV+S) weight ratio of 0.299±0.009 (n=5) compared with 0.257±0.002 (n=4) in the control group (P=0.014; Figure 1C).

DAHP Administration Induces Extensive Pulmonary Arterial Remodeling and Pulmonary Fibrosis

The lungs from DAHP-treated mice were freshly isolated and examined for histological alterations. All of the histological and immunohistochemical data from wild-type (WT) mice, mice of EC-specific DHFR overexpression

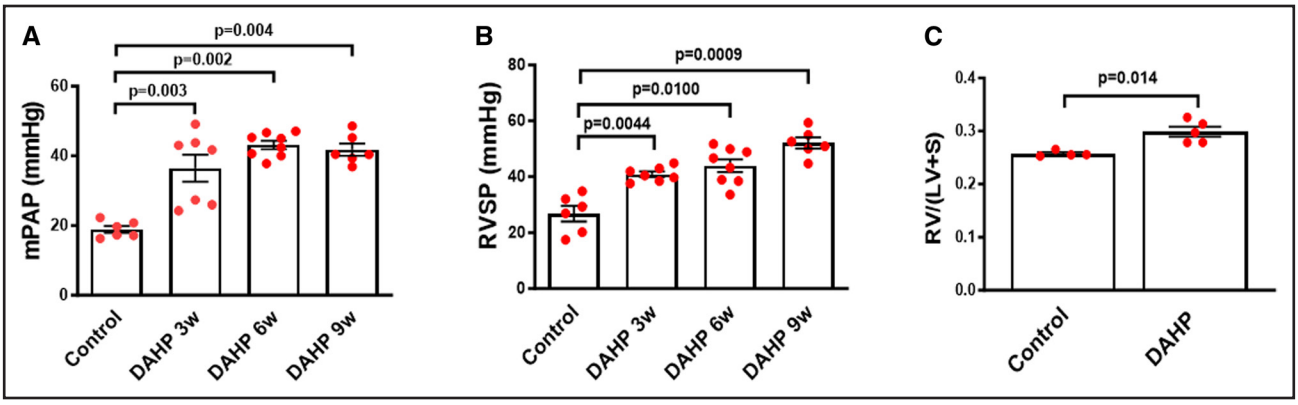

Figure 1. DAHP (2,4-diamino 6-hydroxypyrimidine) treatment induces robust pulmonary hypertension phenotypes in mice: hemodynamics data.

9- to 12-wk-old C57BL/6 male wild-type (WT) mice were exposed to DAHP (10 mmol/L) in the drinking water for 3, 6, and 9 wk. Hemodynamic parameters, including mean pulmonary artery pressure (mPAP) and right ventricular systolic pressure (RVSP), were measured by an open chest method in intubated mice connected to a respirator under anesthesia. **A**, mPAP in control and DAHP-treated groups at different time points, indicating time-dependent elevation in mPAP in response to DAHP treatment. All data are presented as mean±SEM. n=6, 7, 8, and 6 for control, DAHP 3w, DAHP 6w, and DAHP 9w, respectively. P=0.003 for DAHP 3w vs control; P=0.002 for DAHP 6w vs control; and P=0.004 9w vs control. **B**, RVSP in control and DAHP-treated groups at different time points, indicating time-dependent elevation in RVSP in response to DAHP treatment. All data are presented as mean±SEM. n=6, 7, 8, and 6 for control, DAHP 3w, DAHP 6w, and DAHP 9w, respectively. P=0.0044 for DAHP 3w vs control; P=0.0100 for DAHP 6w vs control; and P<0.0009 for DAHP 9w vs control. **C**, Right ventricle (RV)/left ventricle plus septum (LV+S) ratio in control and DAHP-treated groups at 3-wk time point, indicating RVH in response to DAHP treatment. All data are presented as mean±SEM. n=4 and 5 for control and DAHP 3w, respectively. P=0.014 vs control.

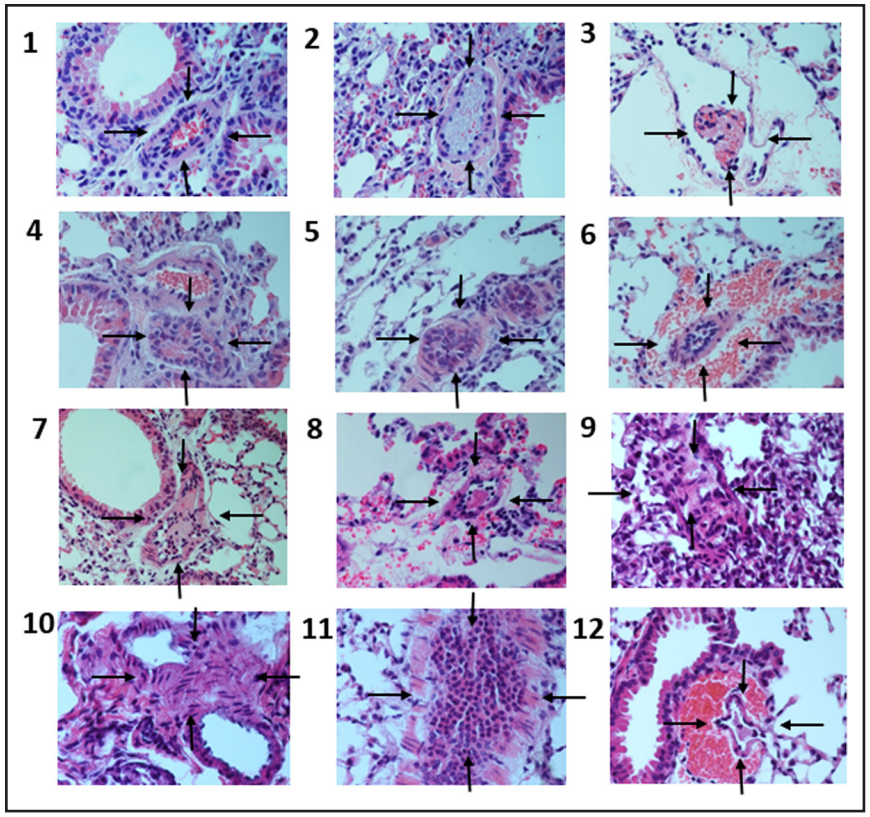

Figure 2. DAHP (2,4-diamino 6-hydroxypyrimidine) treatment induces substantial medial remodeling and formation of a full spectrum of human disease-like vascular lesions in the mouse lung. 9- to 12-wk-old C57BL/6 wild-type (WT) male mice were exposed to DAHP (10 mmol/L) in the drinking water for 9 wks and harvested for histological analysis with Hematoxylin and Eosin Stain (H&E). Black arrows indicate obviously remodeled pulmonary blood vessels. The types of the vascular lesions include (1) media thickening, (2) intima thickening, (3) plexiform lesion (an aneurysm-like pattern), (4) cross-sectional view of an aneurysm-like lesion adjacent to its parent artery, (5) plexiform lesion showing anarchous growth of cells that completely obliterates the vascular lumen, (6) bud-like lesion is covered by an endothelial layer, (7) disorganized stalk-like structures comprising hyperchromatic and oval cells inside the lumen of a pulmonary artery, (8) cross-sectional view of a small pulmonary artery showing a bud-like small cluster of hyperchromatic and oval cells, and (9) to (12) recanalized plexiform lesions.

(tg-EC-DHFR) (Figure 3), and DHFR knockout mice are systematically presented together in Figures 4D-4G and 5A-5F.

Importantly, the DAHP-treated PH mice progressively displayed various types of histological changes in the pulmonary blood vessels that followed features defined at the 6th World Symposium on Pulmonary Hypertension,[47] which simulated human disease. Limited human studies suggest that it takes some time to develop plexiform lesions after the establishment of significantly severe PAH.[48,49] As shown below, mice with early-stage PH (3 weeks after DAHP treatment) displayed medial wall thickening in small pulmonary arteries (<200 μm in diameter). In addition to this change, mice of later-stage PH (9 weeks after DAHP treatment) displayed a full spectrum of vascular lesions as seen in the human disease, including the following (Figure 2): (1) medial thickening, (2) neointima formation/thickening, (3) plexiform lesions (an aneurysm-like pattern), (4) a cross-sectional view of an aneurysm-like lesion adjacent to its parent artery, (5) plexiform lesion showing anarchous growth of cells that completely obliterate the vascular lumen, (6) bud-like lesion covered by an endothelial layer, (7) disorganized stalk-like structures comprising hyperchromatic and oval cells inside the lumen of a pulmonary artery, (8) a cross-sectional view of a small pulmonary artery showing a bud-like small cluster of hyperchromatic and oval cells, and (9) to (12) recanalized lesions.

Transgenesis of DHFR in the Endothelium Protects Against PH in DAHP and Hypoxia Models, While DHFR Knockout Mice Display PH Phenotypes

We and others have demonstrated that endothelial DHFR plays a key role in preserving eNOS coupling activity to attenuate hypertension, aortic aneurysms, and diabetic vascular complications.[21–24,27,32,34–41] We have generated a novel endothelial-specific DHFR transgenic mouse strain (tg-EC-DHFR) to investigate the potential therapeutic effect on PH of endothelial-specific DHFR overexpression in vivo (Figures. 3A-3F). The production construct and the geneotyping results are presented in Figures 3A and 3B respectively. To confirm endothelial-specific transgenesis, we isolated ECs from the aortas and found significant upregulation of DHFR expression in the EC fraction but not in the EC denuded aortic rings (Figures 3C-3D; P=0.0374). Furthermore, immunohistochemical staining also showed EC-specific overexpression of DHFR (Figure 3E), again confirming successful transgenesis of DHFR in ECs in tg-EC-DHFR mice. In addition, tetrahydrobiopterin bioavailability in isolated pulmonary ECs in tg-EC-DHFR mice was markedly increased (Figure 3F; P=0.0326). We did not find any significant differences in body weight, behavior, or activity of the animals compared with WT mice. The tg-EC-DHFR mice were born following a normal gestational period and grew normally into

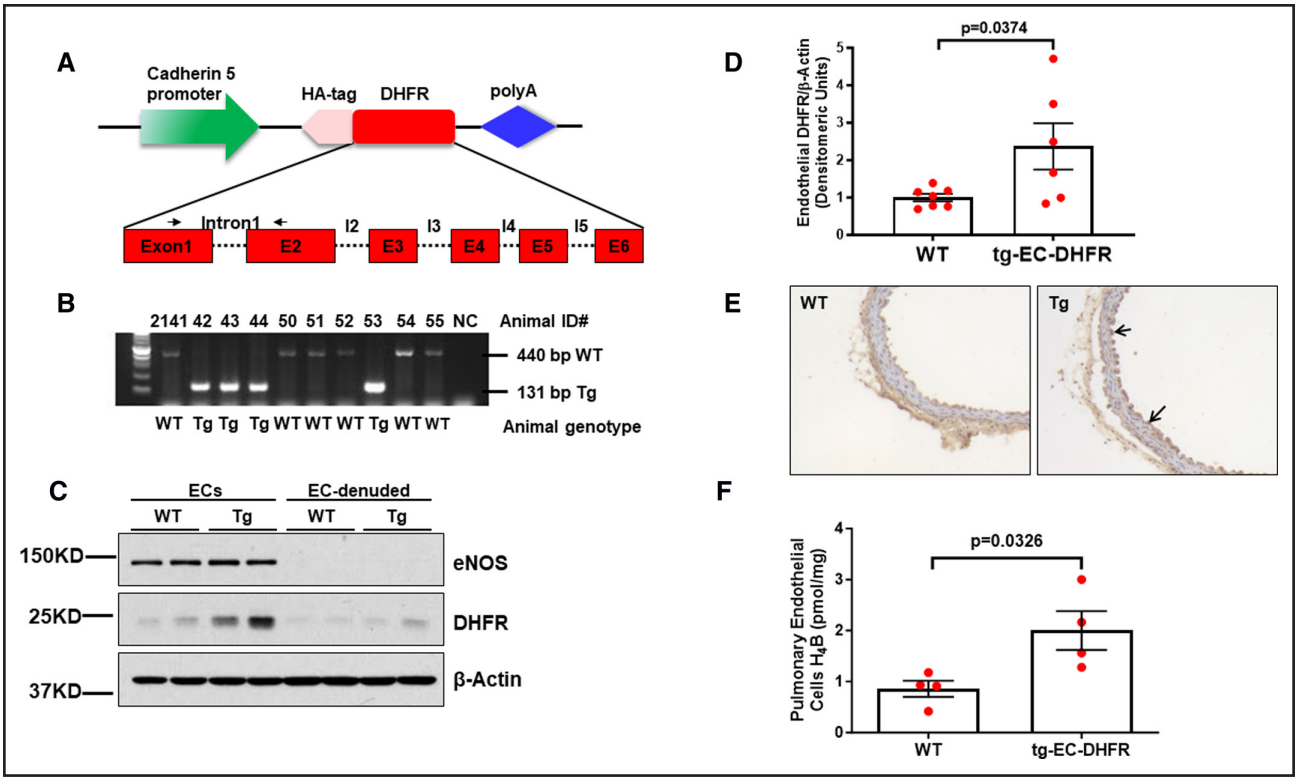

Figure 3. Generation and characterization of endothelial-specific dihydrofolate reductase (DHFR) transgenic mice.
A, Linearized construct including cadherin 5 promoter (endothelial cell [EC] specific), HA-tagged mouse DHFR (coding region), and poly A. Genotyping primers (arrows) were designed to separate DHFR transgene from endogenous DHFR. **B**, Genotyping results from endothelial-specific DHFR transgenic male mice (tg-EC-DHFR) and wild-type (WT) littermates. NC, water as the negative control. **C**, Representative Western blots and quantitative data indicating endothelial-specific overexpression of DHFR in mouse aortas of tg-EC-DHFR mice. eNOS (endothelial nitric oxide synthase) was absent in the denuded aortas indicating successful separation of ECs. **D**, Grouped quantitative data of DHFR expression in aortic EC fractions normalized to β-actin. All data are presented as mean±SEM. n=7 and 6 for WT and tg-EC-DHFR, respectively. *P*=0.0374 for tg-EC-DHFR vs WT control. **E**, Immunohistochemical staining of DHFR in aortic tissues. Arrows indicate enhanced DHFR staining in the endothelial layer of the mouse aortas of the tg-EC-DHFR mice, confirming endothelial-specific overexpression of DHFR. **F**, High-performance liquid chromatography (HPLC) determined tetrahydrobiopterin (H_4B) levels in pulmonary endothelial cells isolated from tg-EC-DHFR mice and WT littermates, indicating functional restoration of H_4B bioavailability in tg-EC-DHFR mice. All data are presented as mean±SEM. n=4 and 4 for WT and tg-EC-DHFR, respectively. *P*=0.0326 for tg-EC-DHFR vs WT control.

adulthood with no detectable abnormalities compared with WT mice.

In addition to formation of human-like vascular lesions as in PH patients (Figure 2), DAHP treated mice developed characteristics of vascular remodeling. In WT mice exposed to DAHP treatment, the medial walls of the pulmonary arterioles were markedly thickened compared with control mice. Consistently, the percentage medial thickness in blood vessels that have an external diameter <200 μm was significantly increased in the DAHP group (58.37±5.76) compared with the control group (25.91±2.96; *P*=0.007 for the DAHP model and *P*=0.019 for the hypoxia model). The percentage medial thickness in blood vessels that have an external diameter of 50 to 100 μm was significantly increased in the DAHP group (71.55±2.56) compared with the control group (33.32±3.89; *P*=0.020). The percentage medial thickness in blood vessels that have an external diameter of 100 to 200 μm was also significantly increased in the DAHP group (54.55±3.17) compared with the control group (30.30±0.05; *P*=0.020).

To investigate the effects of endothelial-specific DHFR overexpression on the development of PH, we assessed the physiological parameters of PH in tg-EC-DHFR mice and WT C57BL/6 mice treated with DAHP (10 mmol/L, 3 weeks) or hypoxia (10% oxygen, 3 weeks). We found that tg-EC-DHFR mice displayed completely attenuated mPAP in response to either DAHP administration or hypoxia treatment (Figure 4A; *P*=0.027 for the DAHP model and *P*=0.033 for the hypoxia model, respectively). The tg-EC-DHFR mice were also protected from developing elevated RVSP (Figure 4B; *P*=0.050 for the DAHP model and *P*=0.088 for the hypoxia model with marginal significance), as well as increased RV/(LV+S) ratio (Figure 4C; *P*=0.047 for the DAHP model and *P*=0.006 for the hypoxia model), in response to either DAHP administration or hypoxia exposure.

In parallel experiments, DHFR knockout mice were generated in-house, as recently published.[36,37] Intriguingly,

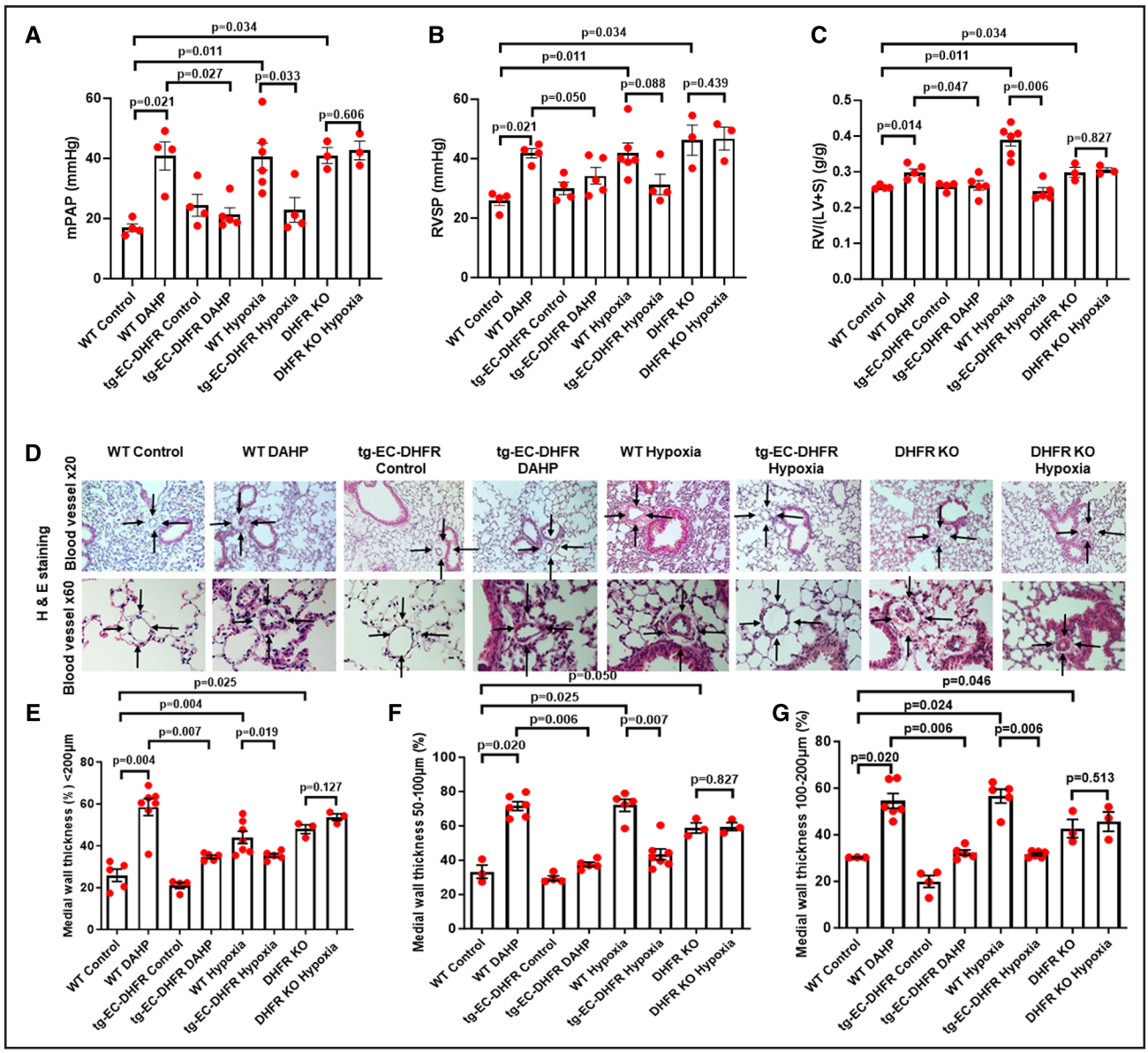

Figure 4. Endothelial-specific overexpression of dihydrofolate reductase (DHFR) in mice protects against development of pulmonary hypertension (PH) and vascular remodeling induced by DAHP (2,4-diamino 6-hydroxypyrimidine) or hypoxia, while DHFR knockout (KO) mice display robust PH phenotypes with no additional deterioration in response to hypoxia exposure. 9- to 12-wk-old wild-type (WT) male mice and tg-EC-DHFR male mice were exposed to DAHP (10 mmol/L) in the drinking water or 10% hypoxia for 3 wk, while DHFR KO mice were exposed to 10% hypoxia for 3 wk. Hemodynamic parameters, including mean pulmonary artery pressure (mPAP) and right ventricular systolic pressure (RVSP), were measured by an open chest method in intubated mice connected to a respirator under anesthesia and then the mice harvested for histological analyses. **A**, mPAP in WT control group, WT DAHP group, tg-EC-DHFR control group, tg-EC-DHFR DAHP group, hypoxia group, tg-EC-DHFR hypoxia group, DHFR KO group, and DHFR KO hypoxia groups. **B**, RVSP in experimental groups as in (**A**). **C**, Right ventricle (RV)/left ventricle plus septum (LV+S) ratio in experimental groups as in (**A**). All data are presented as mean±SEM. For (**A** through **C**), n=4, 4, 4, 5, 6, 4, 3, and 3 for columns from left to right. Precise *P* values are labeled for all comparisons as in the figure. **D**, Representative Hematoxylin and Eosin Stain (H&E) images showing reversal of lung vascular remodeling of medial thickness in tg-EC-DHFR mice exposed to DAHP or hypoxia, and phenotypes of vascular remodeling of medial thickness in DHFR KO mice at baseline and no additional effects with hypoxia exposure. **E**, Percentage medial thickness in vessels <200 µm in external diameter (ED). All data are presented as mean±SEM. n=5, 7, 4, 5, 7, 5, 3, and 3 for columns from left to right. Precise *P* values are labeled for all comparisons as in the figure. **F** and **G**, Percentage medial thickness calculated in differently sized arterioles categorized as 50- to 100-µm ED and 100- to 200-µm ED. All data are presented as mean±SEM. For **F** and **G**, n=3, 6, 4, 5, 5, 7, 3, and 3 for columns from left to right. Precise *P* values are labeled for all comparisons as in the figure.

we found that DHFR knockout mice displayed robust phenotypes of PH as evidenced by elevated levels of mPAP, RVSP, and RV/(LV+S) ratio compared with WT C57BL/6 mice (Figures 4A-4C; *P*=0.034 for mPAP, *P*=0.034 for RVSP, and *P*=0.034 for the RV/(LV+S) ratio, respectively). These data indicate an intrinsic role of DHFR deficiency in the development of PH. Additional features of PH in this strain of mice are described in the following. There are no additional significant changes in mPAP and RVSP in DHFR knockout mice exposed to hypoxia, indicating that DHFR deficiency alone is sufficient to induce a similar PH phenotype as hypoxia, and the responses of hypoxia are mediated intrinsically by DHFR deficiency (Figure 4A and 4B; *P*=0.606 for mPAP and *P*=0.439 for RVSP, indicating no difference between DHFR knockout mice and DHFR knockout mice exposed to hypoxia). Furthermore, hypoxia produced no significant increase in the RV/(LV+S) ratio in DHFR knockout mice (Figure 4C; *P*=0.827).

Transgenesis of DHFR in the Endothelium Prevents Vascular Remodeling in DAHP and Hypoxia Models of PH, While DHFR Knockout Mice Have Extensive Pulmonary Vascular Remodeling

As shown in Figures 4D-4G, the percentage medial thickness was significantly decreased in tg-EC-DHFR mice exposed to DAHP (10 mmol/L, 3 weeks) or hypoxia (10% oxygen, 3 weeks). The percentage medial thickness in <200-µm-diameter blood vessels was markedly attenuated in the tg-EC-DHFR group exposed to DAHP (34.75±0.771) compared with the WT DAHP group (58.44±3.990; Figure 4E; *P*=0.007). The percentage medial thickness in <200-µm-diameter blood vessels in the tg-EC-DHFR group exposed to hypoxia was also significantly abrogated compared with the WT hypoxia group (35.37±0.93 versus 44.02±2.92 for tg-EC-DHFR hypoxia versus WT hypoxia; Figure 4E; *P*=0.019). The percentage medial thicknesses in differently sized diameters of blood vessels in lung tissues are presented separately in Figure 4F and 4G. The percentage medial thickness in 50- to 100-µm-diameter blood vessels in the tg-EC-DHFR group exposed to DAHP (37.54±1.21) was markedly attenuated compared with the WT DAHP group (71.55±2.56; Figure 4F; *P*=0.006). The percentage medial thickness in 50- to 100-µm-diameter blood vessels (43.44±3.15) in the tg-EC-DHFR group exposed to hypoxia was significantly abrogated compared with the WT hypoxia group (72.01±3.52; Figure 4F; *P*=0.007). Similar trends were observed for the percentage medial thickness in 100- to 200-µm-diameter blood vessels in the tg-EC-DHFR group exposed to DAHP (32.33±1.18) compared with the WT DAHP group (54.55±3.17), and for the percentage medial thickness in 100- to 200-µm-diameter blood vessels in the tg-EC-DHFR group exposed to hypoxia (31.62±2.73) compared with the WT hypoxia group (56.60±2.97; Figure 4G; *P*=0.006 and *P*=0.006 for the DAHP model and the hypoxia model, respectively). The tg-EC-DHFR control group showed no significant differences compared with WT controls (Figures 4D-4G).

Of note, DHFR knockout mice (47.95±2.10) showed a significantly increased percentage of medial thickness in <200-µm-diameter blood vessels compared with WT controls (25.91±2.96; Figure 4D and 4E; *P*=0.025). Similarly, the percentage medial thickness in 50- to 100-µm-diameter blood vessels was also much higher in DHFR knockout mice (58.87±2.96) compared with WT controls (33.32±3.89; Figure 4F; *P*=0.050 at marginal significance). The percentage medial thickness in 100- to 200-µm-diameter blood vessels in the DHFR knockout mice was also significantly increased to 42.70±3.91 versus 30.30±0.05 for the WT group (Figure 4G; *P*=0.046). As discussed above, hypoxia had no additional impact on DHFR knockout mice in terms of PH phenotypes featured here for the vascular remodeling (Figures 4D-4G; *P*=0.127, *P*=0.827, and *P*=0.513 for the DHFR knockout hypoxia group comparing with the DHFR knockout group in terms of medial thickness for the groups of <200, 50–100, and 100–200 µm, respectively), indicating an intermediate role for DHFR deficiency in hypoxia-induced PH.

To examine potential lung vascular muscularization and cell proliferation in DAHP-treated mice, lung sections were stained with antibodies specific for SMA (smooth muscle α-actin) and PCNA (proliferative cell nuclear antigen; for proliferating cells). Immunohistological analysis of lung tissues revealed vascular muscularization as evidenced by increased SMA-positive staining in DAHP-treated mouse pulmonary arterioles. The fluorescent intensity of SMA in the lung sections was significantly increased in the DAHP group (32.36±1.36) compared with the control group (17.01±2.12; Figure 5A and 5B; *P*=0.034). Likewise, the fluorescent intensity of PCNA was markedly elevated in the DAHP group (24.30±1.62) compared with the control group (11.97±2.54; Figure 5A and 5B; *P*=0.021), indicating increased cell proliferation.

The expression of SMA by DAB staining in the lung sections was also significantly increased in the DAHP group (9.35±0.39 versus 2.73±0.07 for the DAHP group versus the control group; *P*=0.011; Figure 5C and 5D). A similar trend was seen for PCNA using DAB staining (5.98±0.99 versus 0.80±0.05 for the DAHP group versus the control group), as shown in Figure 5C and 5D (*P*=0.021). In addition, collagen deposition as assessed by Masson trichrome staining was found to be markedly increased in the peribronchial and perivascular areas in the DAHP-treated mouse lung tissue sections (12.74±0.53 versus 3.82±0.61 for the DAHP group versus control group; Figure 5E and 5F; *P*=0.009).

Similar to the attenuating effects on mPAP, RVSP, and RV/(LV+S) ratio as discussed earlier, the increased

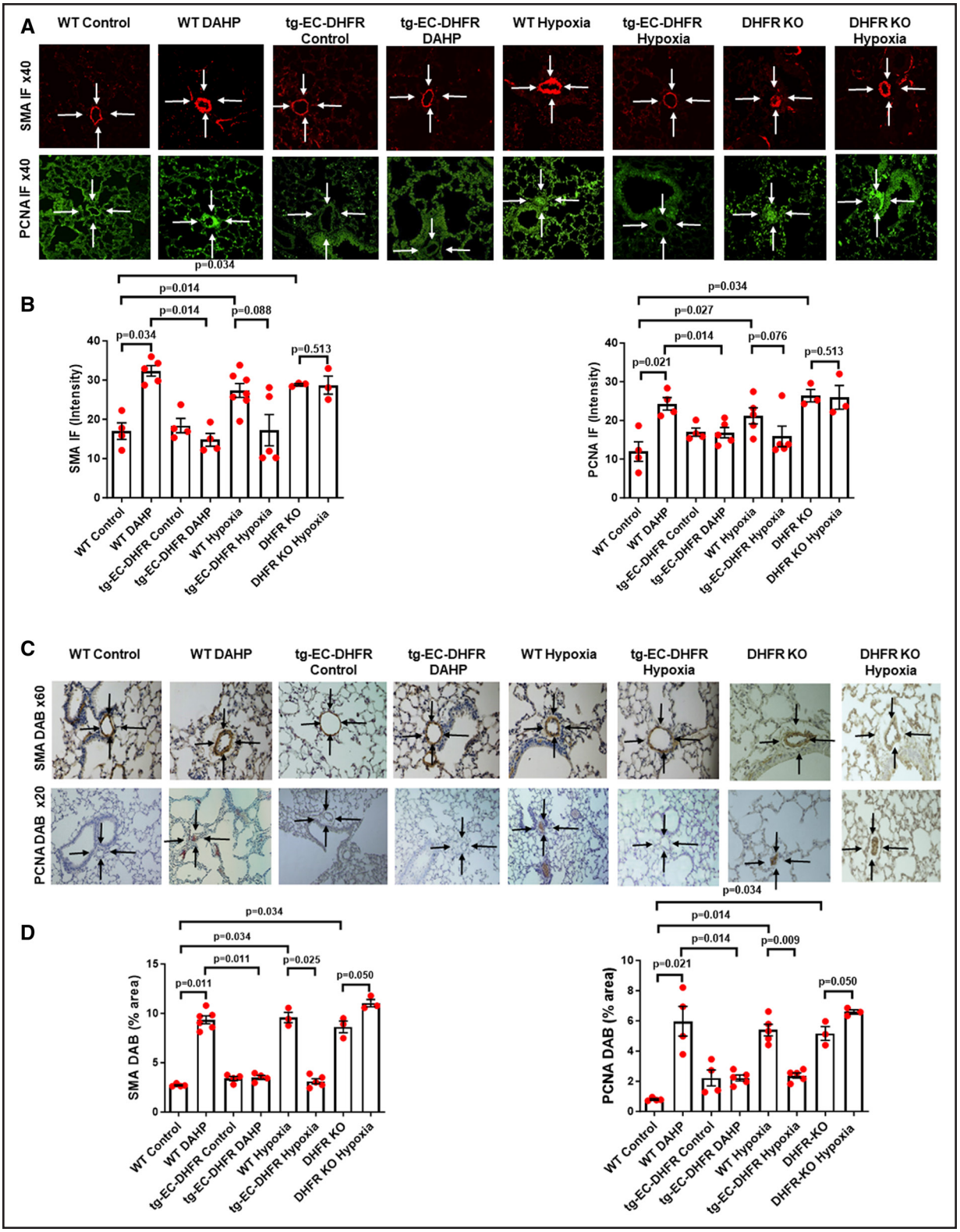

Figure 5. Endothelial-specific overexpression of dihydrofolate reductase (DHFR) in mice prevents cell proliferation, muscularization, and fibrosis of pulmonary blood vessels in DAHP (2,4-diamino 6-hydroxypyrimidine) and hypoxia-induced pulmonary hypertension models, while DHFR knockout (KO) mice display features of extensive vascular remodeling with no additional responses to hypoxia exposure.

9- to 12-wk-old wild-type (WT) male mice and tg-EC-DHFR male mice were exposed to DAHP (10 mmol/L) in the drinking water or 10% hypoxia for 3 wk, while DHFR KO male mice were exposed to 10% hypoxia for 3 wk. At the end of the experimental protocol, mice were harvested for immunofluorescent and immunohistochemical analyses with corresponding antibodies for determination of SMA (smooth muscle α-actin) or PCNA (proliferative cell nuclear antigen) expression, and Masson's trichrome staining for assessment of fibrosis. **A**, (*Continued*)

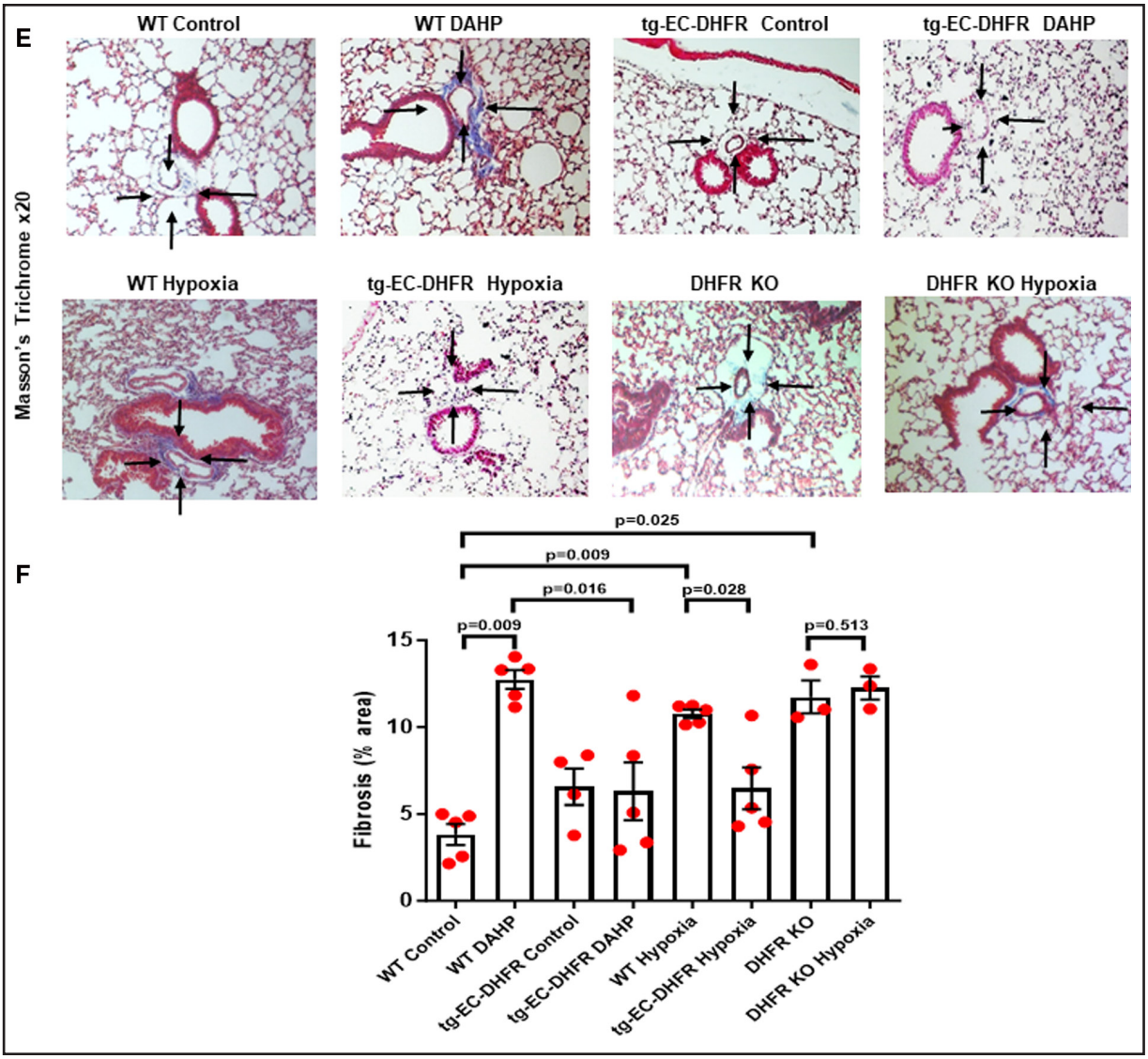

Figure 5 Continued. Representative images of pulmonary blood vessels immunostained for SMA (red) and PCNA (green) with immunofluorescent antibodies (×40 magnification). **B**, Quantification of fluorescent intensity of SMA and PCNA expression in lung sections of each experimental group. All data are presented as mean±SEM. n=4, 5, 4, 4, 7, 5, 3, and 3 for columns from left to right for SMA expression. n=4, 4, 4, 5, 5, 5, 3, and 3 for columns from left to right for PCNA expression. Precise *P* values are labeled for all comparisons as in the figure. **C**, Representative images of pulmonary blood vessels immunostained for SMA and PCNA using 3, 3 -diaminobenzidine (DAB) substrate (brown; ×60 and ×20 magnifications). **D**, Quantification of percentage area (DAB) of SMA and PCNA expression in lung sections of each experimental group. All data are presented as mean±SEM. n=4, 6, 4, 4, 3, 5, 3, and 3 for columns from left to right for SMA expression. n=4, 4, 4, 5, 5, 5, 3, and 3 for columns from left to right for PCNA expression. Precise *P* values are labeled for all comparisons as in the figure. **E**, Representative images of Masson's trichrome staining show collagen deposition (blue) in perivascular and peribronchial areas of lung sections of each experimental group. **F**, Percentage fibrosis in lung sections of each experimental group. All data are presented as mean±SEM. n=5, 5, 4, 5, 5, 5, 3, and 3 for columns from left to right for collagen deposition. Precise *P* values are labeled for all comparisons as in the figure.

expression of SMA and PCNA in the DAHP model was abrogated in lung sections of tg-EC-DHFR mice exposed to DAHP (Figures 5A-5D, *P*=0.014 for SMA IF, *P*=0.014 for PCNA IF, *P*=0.011 for SMA-DAB, and *P*=0.014 for PCNA DAB, respectively). Likewise, the increased expression of SMA and PCNA in the hypoxia model was attenuated in lung sections of tg-EC-DHFR mice exposed to hypoxia (Figures 5A-5D, *P*=0.088 for SMA IF, *P*=0.076 for PCNA IF with marginal significance, *P*=0.025 for SMA-DAB, and *P*=0.009 for PCNA DAB, respectively). However, the expression of SMA and PCNA was increased in lung sections of DHFR knockout mice compared with WT controls (Figures 5A-5D; *P*=0.034 for SMA IF, *P*=0.034 for PCNA IF, *P*=0.034 for SMA-DAB, and *P*=0.034 for PCNA DAB, respectively). Similar to the observations above, DHFR knockout mice exposed to hypoxia showed no additional regulations compared with unexposed DHFR knockout mice at

baseline, indicating that DHFR deficiency mediates these characteristic changes in the hypoxia model. Consistently, Masson's trichrome staining for collagen deposition indicated decreased fibrosis in the perivascular and peribronchial areas of the lung sections of tg-EC-DHFR mice after DAHP or hypoxia exposure compared with the corresponding WT groups (Figure 5E and 5F; P=0.016 for the DAHP model and P=0.028 for the hypoxia model). By contrast, increased fibrosis in the perivascular and peribronchial areas of the lung sections was observed in DHFR knockout mice (Figure 5E and 5F; P=0.025), while no additional changes in DHFR knockout mice exposed to hypoxia (Figure 5E and 5F; P=0.513).

Taken together, these data demonstrate a robust and innovative protective role of endothelium-specific DHFR overexpression in preserving vascular structure and function to attenuate vascular remodeling and PH development in both DAHP and hypoxia models of PH. Complementarily, a deficiency in DHFR is intrinsically causal to vascular remodeling and PH.

DAHP Administration Reduces NO Bioavailability and Increases total Superoxide and Mitochondrial Superoxide Production

Endothelial NO bioavailability was assessed in mouse lungs in situ by fluorescent imaging using the NO-specific fluorescent probe 4-Amino-5-Methylamino-2',7'-Difluorofluorescein Diacetate (DAF-FM DA). The image analysis of lung sections stained with DAF-FM

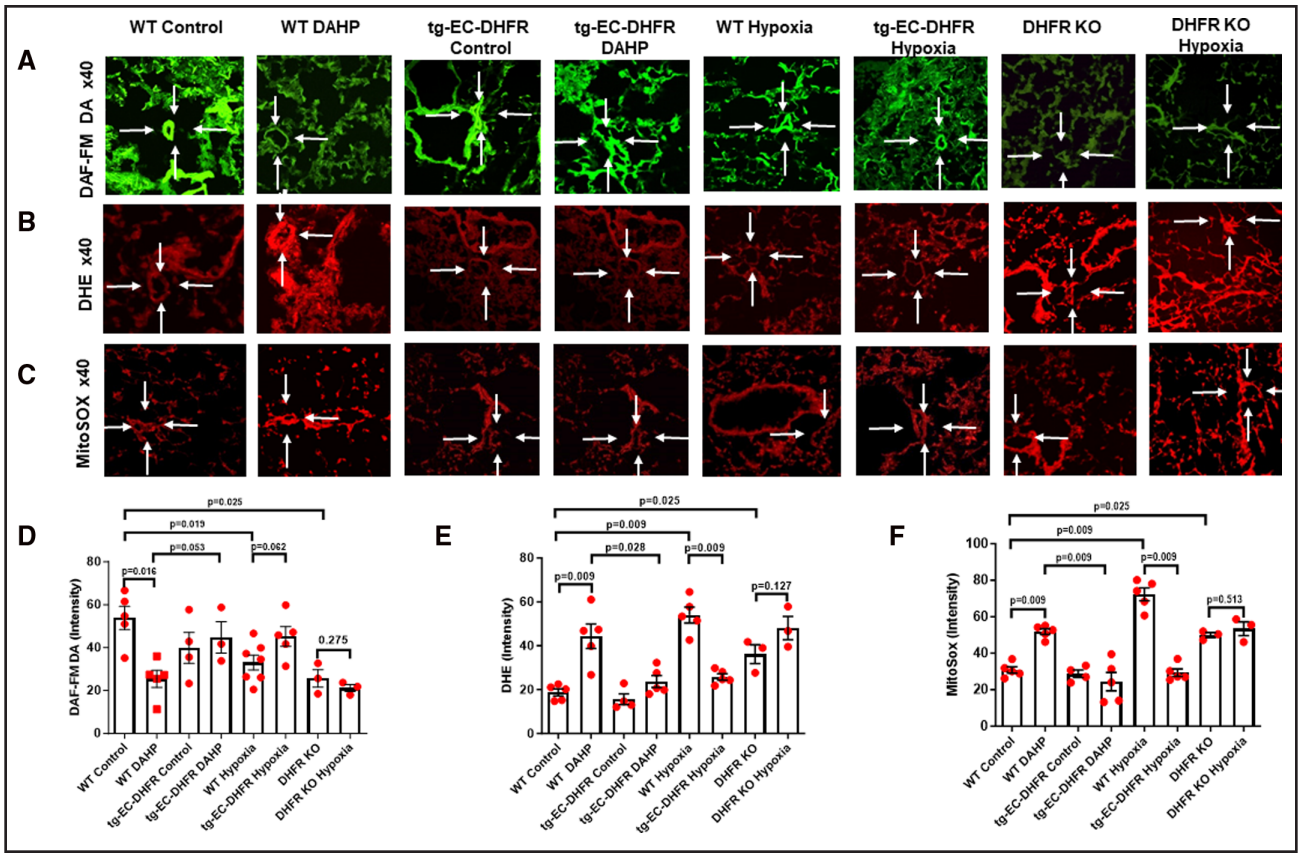

Figure 6. Endothelial-specific overexpression of dihydrofolate reductase (DHFR) in mice prevents nitric oxide (NO) deficiency and increased total and mitochondrial superoxide production, while DHFR knockout (KO) mice display features of increased total and mitochondrial superoxide production and reduced NO bioavailability as in DAHP (2,4-diamino 6-hydroxypyrimidine)–treated mice and show no additional effects with hypoxia exposure.

9- to 12-wk-old wild-type (WT) male mice and tg-EC-DHFR male mice were exposed to DAHP (10 mmol/L) in the drinking water or 10% hypoxia for 3 wk, while DHFR KO male mice were exposed to 10% hypoxia for 3 wk. At the end of the experimental protocol, mice were harvested for analyses of NO bioavailability, and total and mitochondrial superoxide production. Representative images of fluorescent signals of (**A**) 4-Amino-5-Methylamino-2',7'-Difluorofluorescein Diacetate (DAF-FM DA) for NO, (**B**) Dihydroethidium (DHE) for total superoxide, and (**C**) MitoSOX for mitochondrial superoxide, in WT and tg-EC-DHFR mice treated with DAHP or hypoxia, and in DHFR KO mice with and without hypoxia exposure. **D**, Quantitative data of DAF-FM DA fluorescent signals. All data are presented as mean±SEM. n=5, 5, 4, 3, 7, 5, 3, and 3 for columns from left to right. Precise P values are labeled for all comparisons as in the figure. **E**, Quantitative data of DHE fluorescent signals. All data are presented as mean±SEM. n=5, 5, 4, 5, 5, 5, 3, and 3 for columns from left to right. Precise P values are labeled for all comparisons as in the figure. **F**, Quantitative data of MitoSOX fluorescent signals. All data are presented as mean±SEM. n=5, 5, 4, 5, 5, 5, 3, and 3 for columns from left to right. Precise P values are labeled for all comparisons as in the figure.

DA showed decreased NO bioavailability in the DAHP group (25.32±2.78 versus 53.82±5.39 for the DAHP group versus control group; Figures 6A and 6D; *P*=0.016). We next determined the effects of DAHP on total and mitochondrial superoxide production in lung tissue sections. Total superoxide in lung tissue sections was determined using dihydroethidium (DHE) fluorescent imaging. DHE staining detects intracellular superoxide, which has been further validated using electron spin resonance (ESR) in the following. Results shown in Figures 6B and 6E indicate that the DHE fluorescent intensity was markedly increased in the DAHP group (44.39±5.57) compared with the control group (18.78±1.58, *P*=0.009).

We have previously shown that the mitochondrion lies downstream of uncoupled eNOS to mediate the development of hypertension and aortic aneurysm.[36,37] To evaluate mitochondrial dysfunction and its potential contribution to the enhanced intracellular superoxide generation in the lung tissue of PH mice, mitochondrial superoxide generation was detected using MitoSOX red fluorescent probe. As shown in Figures 6C and 6F, DAHP treatment significantly increased mitochondrial superoxide production in the lung (51.78±1.58 versus 30.78±1.76 for the DAHP group versus the control group; *P*=0.009). These results indicate increased mitochondrial ROS production downstream of uncoupled eNOS, which was accompanied by reduced NO bioavailability.

Transgenesis of DHFR in the Endothelium Preserves NO Bioavailability While Reducing Superoxide Generation in DAHP and Hypoxia Models of PH

Transgenesis of DHFR is anticipated to reverse eNOS uncoupling, which will lead to restored NO bioavailability. Therefore, we next determined effects of DHFR transgenesis on NO bioavailability in lung tissue sections. As shown in Figures 6A-6F, fluorescent staining was utilized to detect NO production (DAF-FM DA), total superoxide (DHE) and mitochondrial superoxide production (MitoSOX). Compared with the DAHP- or hypoxia-treated WT group, the NO fluorescent intensity was much higher in the tg-EC-DHFR mice exposed to either DAHP or hypoxia (Figures 6A and 6D; *P*=0.053 for the DAHP model and *P*=0.062 for the hypoxia model with marginal significance). DHFR knockout mice, however, displayed significantly lower NO fluorescent intensity (Figures 6A and 6D; *P*=0.025). Of note, DAF-FM DA fluorescent imaging labels diffusible NO at various locations of different cell types, among which only the staining on blood vessels/ECs is relevant to vascular regulations and implications in the development of PH. In contrast, quantitative analyses of DHE and MitoSOX fluorescent imaging of lung sections from tg-EC-DHFR DAHP and tg-EC-DHFR hypoxia groups showed decreased levels of total and mitochondrial superoxide production compared with the corresponding WT groups (Figures 6B, 6C, 6E and 6F; *P*=0.028 and *P*=0.009 for comparison of DHE intensities in DAHP and hypoxia models, respectively, and *P*=0.009 and *P*=0.009 for comparison of MitoSOX intensities in DAHP and hypoxia models, respectively), indicating protective effects of endothelium-targeted DHFR transgenesis on eNOS/endothelial function. Of note, DHFR knockout mice showed significantly higher DHE and MitoSOX fluorescent intensities and lowered DAF-FM DA fluorescent intensity for increased superoxide production and reduced NO bioavailability (Figures 6A-6F; *P*=0.025 for comparison of DHE intensities and *P*=0.025 for comparison of MitoSOX intensities). In addition, we observed eNOS uncoupling activity in both DAHP and hypoxia models of PH by electron spin resonance (ESR) analysis, as shown in Figures 7A-7B and described in the following. The tetrahydrobiopterin bioavailability determined by high-performance liquid chromatography (HPLC) was also deficient in DAHP and hypoxia-treated mice (Figures 7A-7B).

Transgenesis of DHFR in the Endothelium Restores Tetrahydrobiopterin Bioavailability and Recouples eNOS in DAHP and Hypoxia Models of PH

DAHP administration inhibits GTPCHI to induce tetrahydrobiopterin deficiency and subsequent uncoupling of eNOS. Under normal conditions when eNOS is coupled, the addition of the eNOS inhibitor L-NG-Nitro arginine methyl ester (L-NAME) will increase the measured superoxide production, as eNOS is producing NO to scavenge superoxide; however, when eNOS is uncoupled and producing superoxide, its inhibition will lead to a decrease in measured superoxide. We, therefore, examined whether eNOS was uncoupled in DAHP-induced PH in mice and whether endothelial-specific overexpression of DHFR recoupled eNOS in both DAHP and hypoxia models of PH. Electron spin resonance was used to examine eNOS uncoupling activity as previously published,[21–41] in DAHP - and hypoxia-treated WT mice, and tg-EC-DHFR mice (Figure 7A), as well as in DHFR knockout control mice and DHFR knock out mice exposed to hypoxia (Figure 7A). While eNOS uncoupling activity was markedly increased in DAHP (superoxide levels: 19.63±3.13-µmol/L per min/mg protein) or hypoxia-exposed groups (29.33±3.63-µmol/L per min/mg protein) compared with controls (9.00±0.28-µm/min per mg protein), it was completely reversed in tg-EC-DHFR control (12.03±1.84-µmol/L per min/mg protein), tg-EC-DHFR DAHP (5.20±0.28-µmol/L per min/mg protein), and tg-EC-DHFR hypoxia (9.70±1.98-µmol/L per min/mg protein) groups (Figure 7A). The measurements made without L-NAME, shown in white bars with red dots, indicate that DAHP

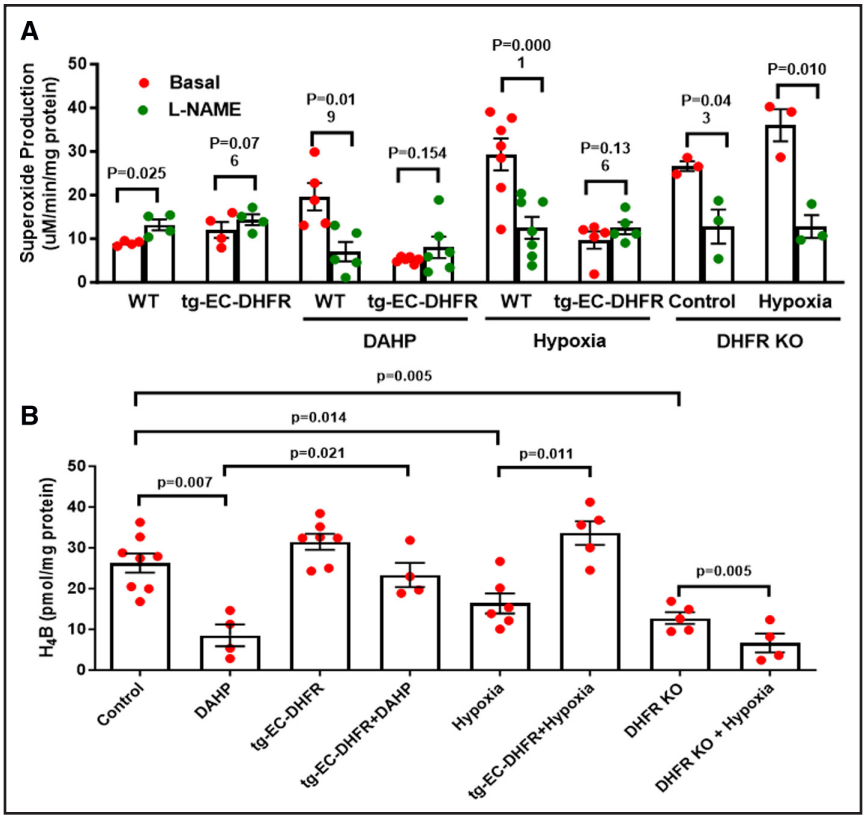

Figure 7. Endothelial-specific overexpression of dihydrofolate reductase (DHFR) restores tetrahydrobiopterin (H_4B) bioavailability and recouples eNOS (endothelial nitric oxide synthase) in DAHP (2,4-diamino 6-hydroxypyrimidine) and hypoxia-induced pulmonary hypertension models.

9- to 12-wk-old wild-type (WT) male mice and tg-EC-DHFR male mice were exposed to DAHP (10 mmol/L) in the drinking water or 10% hypoxia for 3 wk, while DHFR knockout (KO) male mice were exposed to 10% hypoxia for 3 wk. At the end of the experimental protocol, mice were harvested for high-performance liquid chromatography (HPLC) determination of H_4B bioavailability and electron spin resonance (ESR) determination of eNOS uncoupling activity. **A**, ESR determined eNOS uncoupling activity in WT mice and tg-EC-DHFR mice exposed to DAHP or hypoxia, indicating prevention of eNOS uncoupling in DAHP or hypoxia-treated tg-EC-DHFR mice. eNOS was also uncoupled in DHFR KO mice at baseline with no significant additional effects in response to hypoxia exposure. All data are presented as mean±SEM. n=4, 4, 4, 4, 5, 5, 6, 6, 7, 7, 5, 5, 3, and 3 for columns from left to right. Precise *P* values are labeled for all comparisons as in the figure. L-NG-Nitro arginine methyl ester (L-NAME). **B**, HPLC determined H_4B bioavailability in lung tissues of WT mice and tg-EC-DHFR mice exposed to DAHP or hypoxia, indicating preservation of H_4B bioavailability in DAHP or hypoxia-treated tg-EC-DHFR mice, and in WT mice and DHFR KO mice exposed to hypoxia, indicating H_4B deficiency in DHFR KO mice and modest additional effects with hypoxia that matches minor additional uncoupling of eNOS in DHFR KO mice. All data are presented as mean±SEM. n=8, 4, 7, 4, 6, 5, 5, and 4 for columns from left to right. Precise *P* values are labeled for all comparisons as in the figure.

treatment or hypoxia exposure significantly increased total superoxide production in the WT lung tissue samples (*P*=0.019 and *P*=0.0001 for DAHP and hypoxia groups, respectively). The measurements made with L-NAME, as shown in the white bars with green dots, are performed to assess the uncoupling state of eNOS. These data indicate that eNOS uncoupling activity in the lung, as reflected by L-NAME-dependent superoxide production, was significantly increased in both DAHP and hypoxia models of PH. These phenotypes were completely reversed in tg-EC-DHFR groups exposed to DAHP or hypoxia because measurements in the presence no longer indicates a significant amount of superoxide production (*P*=0.154 or *P*=0.136 for tg-EC-DHFR mice exposed to DAHP or hypoxia). Notably, similar to other features of PH described above, DHFR knockout mice displayed L-NAME sensitive eNOS uncoupling activity at baseline (*P*=0.043), indicating an intrinsic role of DHFR deficiency in PH development.

The upregulation in endothelial DHFR in tg-EC-DHFR mice is anticipated to result in improved tetrahydrobiopterin bioavailability and recoupling of eNOS via DHFR-dependent regeneration of tetrahydrobiopterin. We, therefore, determined levels of bioavailable tetrahydrobiopterin using HPLC. While tetrahydrobiopterin bioavailability was markedly diminished in DAHP treated group (8.54±2.70-pmol/mg protein) or hypoxia-exposed group (16.38±2.48-pmol/mg protein) compared with controls (26.29±2.36-pmol/mg protein; *P*=0.007 or *P*=0.014 for DAHP or hypoxia group), it was completely preserved in tg-EC-DHFR controls (31.48±1.94-pmol/mg protein), tg-EC-DHFR DAHP (23.35±2.97-pmol/

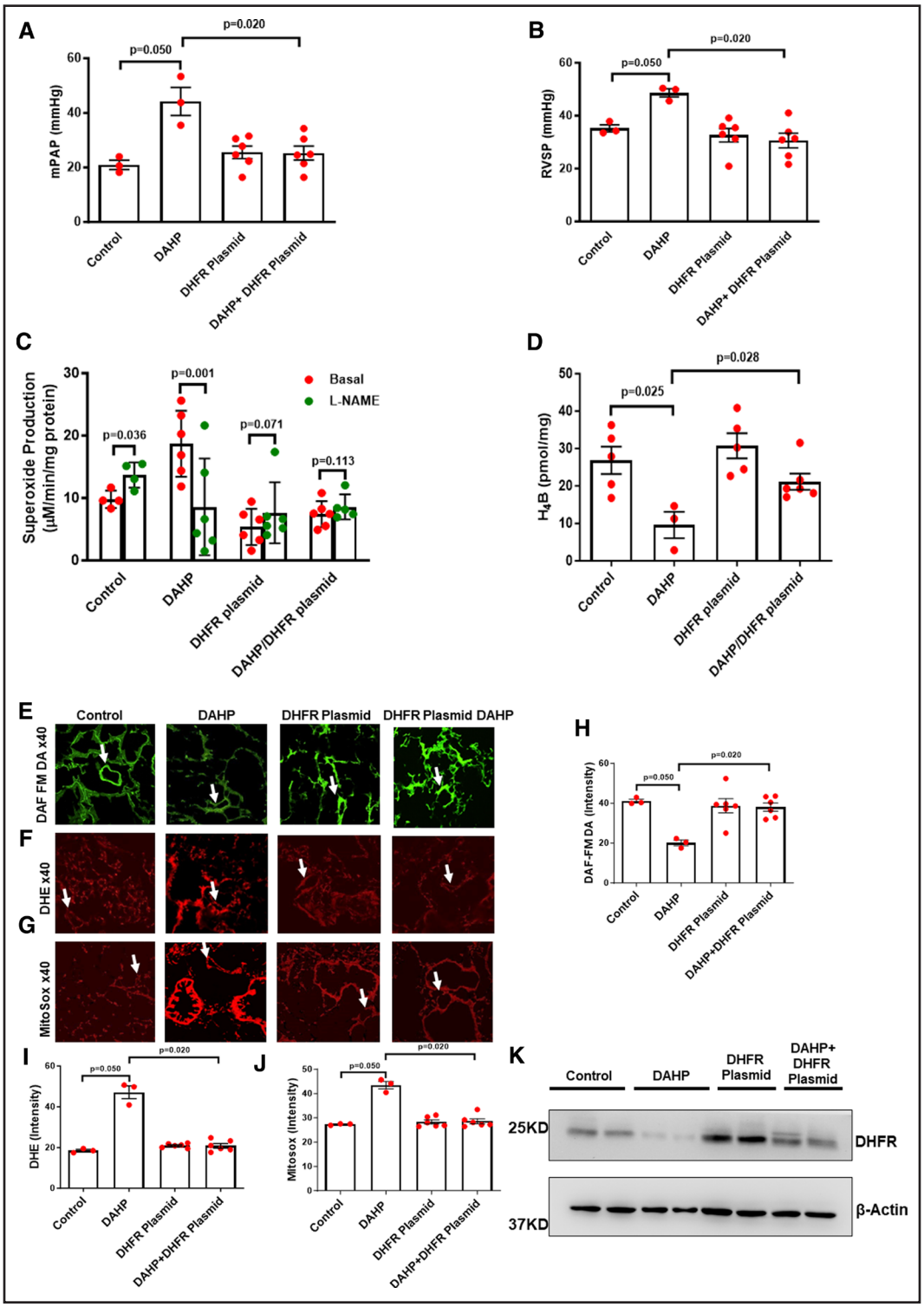

Figure 8. Overexpression of dihydrofolate reductase (DHFR) after initiation of pulmonary hypertension (PH) reverses PH development in DAHP (2,4-diamino 6-hydroxypyrimidine)-treated mice.

9- to 12-wk-old wild-type (WT) C57BL/6 mice were injected with pCMV-DHFR plasmid every other day from the eighth day after the first DAHP treatment and harvested after 3 wk. **A**, Mean pulmonary artery pressure (mPAP) in control and DHFR plasmid–treated groups that were exposed to DAHP, indicating the reversal of PH phenotype by DHFR overexpression after initiation of PH. All data are presented as mean±SEM. n=3, 3, 6, and 6 for columns from left to right. **B**, Right ventricular systolic pressure (RVSP) in control and DHFR plasmid–treated groups that were exposed to DAHP, indicating reversal of PH phenotype by DHFR overexpression after initiation of PH. All data are presented as mean±SEM. n=3, 3, 6, and 6 for columns from left to right. Precise *P* values are labeled (*Continued*)

mg of protein; *P*=0.021 versus WT DAHP group), and tg-EC-DHFR hypoxia (33.63±2.89-pmol/mg of protein; *P*=0.011 versus WT hypoxia group) groups (Figure 7B). This restoration was accompanied by the complete recoupling of eNOS in these animals (Figure 7A). Data in Figure 7B also indicate reduced levels of tetrahydrobiopterin in DHFR knockout mice (12.75±1.44-pmol/mg protein; *P*=0.005).

Reversal of PH by Overexpression of DHFR After Initiation of DAHP Treatment

We have performed additional experiments to overexpress DHFR in the DAHP model after initiation of PH and found that it was markedly effective in fully reversing the PH phenotypes. WT C57BL/6 mice were injected (iv) of pCMV-DHFR plasmid from the eighth day after the first DAHP treatment, and the mice were injected every other day till harvest at the end of 3 weeks. As shown in Figure 8A, mPAP was substantially increased in mice treated with 10-mmol/L DAHP for 3 weeks (20.95±1.66 versus 44.22±5.17 mm Hg for control versus DAHP; *P*=0.050). This effect was fully reversed in mice injected with pCMV-DHFR plasmid to overexpress DHFR (25.30±2.59 versus 44.22±5.16 mm Hg for pCMV-DHFR plasmid with DAHP versus DAHP; *P*=0.020; Figure 8A). Likewise, as shown in Figure 8B, RVSP was substantially increased in mice treated with 10-mmol/L DAHP for 3 weeks (35.22±1.66 versus 48.63±5.17 mm Hg for control versus DAHP; *P*=0.050 with marginal significance). This effect was fully reversed in mice injected with pCMV-DHFR plasmid to overexpress DHFR (30.60±2.31 versus 48.63±5.17 mm Hg for pCMV-DHFR plasmid with DAHP versus DAHP; *P*=0.020).

Data in Figure 8C indicate that eNOS uncoupling activity was increased in mice treated with DAHP for 3 weeks (9.80±0.70-µmol/L per min/mg protein versus 18.71±2.16-µmol/L per min/mg protein for control versus DAHP). This effect was fully reversed in mice injected with pCMV-DHFR plasmid to overexpress DHFR (5.38±1.18-µmol/L per min/mg protein versus 18.71±2.16-µmol/L per min/mg protein for pCMV-DHFR plasmid control versus DAHP) and mice injected with pCMV-DHFR plasmid that exposed to DAHP (7.42±0.85 versus 18.71±2.16 for pCMV-DHFR plasmid with DAHP versus DAHP). Likewise as described earlier, L-NAME (L-NG-Nitro arginine methyl ester) sensitive superoxide production/eNOS uncoupling activity was documented in the DAHP group (*P*=0.001), while this response was fully reversed in mice overexpressed DHFR with pCMV-DHFR plasmid (*P*=0.113 for no difference between conditions with/without L-NAME) (Figure 8C). In the control group, L-NAME inhibits NO production from coupled eNOS, resulting in increased measurable superoxide (*P*=0.036). We also determined the levels of bioavailable tetrahydrobiopterin using HPLC. While the tetrahydrobiopterin levels were markedly diminished in the DAHP group, it was completely preserved in the pCMV-DHFR plasmid-treated group (Figure 8D). Tetrahydrobiopterin was substantially decreased in mice treated with DAHP for 3 weeks (26.83±3.64 versus 9.59±3.51 pmol/mg of protein for control versus DAHP; *P*=0.025). This effect was fully reversed in mice injected with the pCMV-DHFR plasmid to overexpress DHFR (21.15±2.16 versus 9.59±3.51 pmol/mg of protein for pCMV-DHFR plasmid with DAHP versus DAHP; *P*=0.028) Figure 8D. As shown in Figures 8E and 8H, NO bioavailability was also fully restored by DHFR overexpression after initiation of PH (*P*=0.050 for DAHP versus control and *P*=0.020 for pCMV-DHFR plasmid with DAHP versus DAHP), while total and mitochondrial superoxide levels were fully attenuated by DHFR overexpression after initiation of PH (Figures 8F and 8I for total superoxide production, *P*=0.050 for DAHP versus control with marginal difference, and *P*=0.020 for pCMV-DHFR plasmid with DAHP versus DAHP; and Figures 8G and 8J for total mitochondrial superoxide production, *P*=0.050 for DAHP versus control with marginal difference, and *P*=0.020 for pCMV-DHFR plasmid with DAHP versus DAHP). Indeed, in these mice, DHFR was successfully overexpressed in the lung tissues as shown in the representative Western blot (Figure 8K).

Figure 8 Continued. for all comparisons as in the figure. **C**, Electron spin resonance determined eNOS (endothelial nitric oxide synthase) uncoupling activity in control and DHFR plasmid–treated groups that were exposed to DAHP, indicating reversal of eNOS uncoupling by DHFR overexpression after initiation of PH. All data are presented as mean±SEM. n=4, 4, 6, 6, 6, 6, 6, and 6 for columns from left to right. Precise *P* values are labeled for all comparisons as in the figure. **D**, HPLC determined tetrahydrobiopterin (H_4B) bioavailability in lung tissues of control and DHFR plasmid–treated groups that were exposed to DAHP, indicating reversal of H_4B bioavailability by DHFR overexpression after initiation of PH. All data are presented as mean±SEM. n=5, 3, 5, and 6 for columns from left to right. Precise *P* values are labeled for all comparisons as in the figure. Shown are representative images of fluorescent signals of (**E**) DAF-FM DA, (**F**) DHE, and (**G**) MitoSOX staining for the detection of nitric oxide (NO) production (green) and total and mitochondrial superoxide generation (red), respectively, in control and DHFR plasmid–treated groups that were exposed to DAHP. **H**, Quantitative data of DAF-FM DA fluorescent signals. All data are presented as mean±SEM. **I**, Quantitative data of DHE fluorescent signals. All data are presented as mean±SEM. n=3, 3, 6, and 6 for columns from left to right. Precise *P* values are labeled for all comparisons as in the figure. **J**, Quantitative data of MitoSOX fluorescent signals. All data are presented as mean±SEM. n=3, 3, 6, and 6 for columns from left to right. Precise *P* values are labeled for all comparisons as in the figure. These data indicate the reversal of NO deficiency and increased total and mitochondrial superoxide generation by DHFR overexpression after initiation of PH. **K**, Representative Western blots indicating DHFR was successfully overexpressed in the lung tissues by transfection with DHFR plasmid.

RNA-Sequencing Analysis in DAHP and Hypoxia Models of PH and Patients With PH Indicates a Greatly More Similar Gene Regulation Profile Between the DAHP Model and the Human PH

To compare the DAHP model with the hypoxia model in regard to their resemblance to human PH, we analyzed the transcriptomes of lung tissues isolated from both mouse models of PH and human patients with PH using RNA-seq. We collected lung tissues from 10 healthy control donors (8 men and 2 women, aged 44.0±3.3 years) and lung explants from 12 patients with pulmonary arterial hypertension (PAH) (undergoing lung transplantation at the China-Japan Friendship Hospital: 9 men and 3 women, aged 57.6±3.5 years; echo estimated sPAP, 63.41±5.71 mm Hg). As shown in Figure 9, 4548 differentially expressed genes (DEGs) were identified in patients with PH compared with donor controls. We collected lung tissues for RNA-seq from control, DAHP-treated, and hypoxia-exposed mice (3 animals for each group). Compared with the control mice, hypoxia treatment induced 439 DEGs in mice, 123 of which overlapped with human DEGs (Figure 9). Three weeks of DAHP treatment resulted in 733 DEGs in mice, 325 of which overlapped with human DEGs (Figure 9). In addition, we identified 23 DEGs that are common among the 3 comparative groups of human PAH, and DAHP and hypoxia models of PH. Based on the results of Ingenuity Pathway Analysis (QIAGEN), we grouped the 325 DEGs into different disease and function-related pathways. These data clearly demonstrate that the mouse DAHP model shares greatly more DEGs with human PH than the hypoxia model.

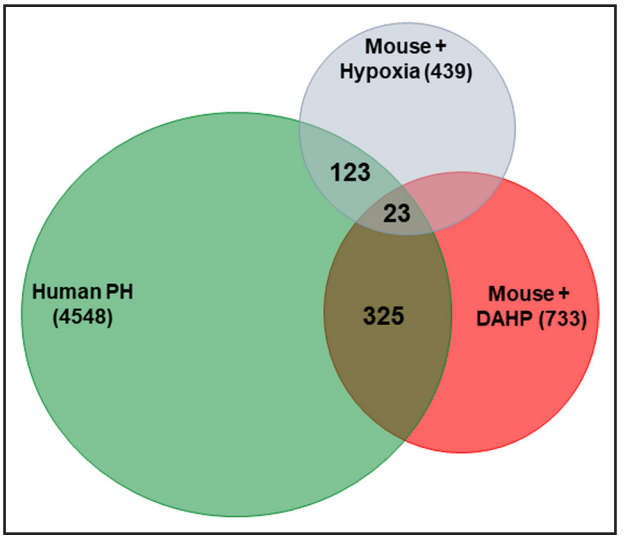

Figure 9. Venn diagram illustrating the total number and the overlap of differentially expressed genes (DEGs) identified from RNA-seq analyses of lung tissues from patients with pulmonary hypertension (PH) and from DAHP (2,4-diamino 6-hydroxypyrimidine) and hypoxia-treated mouse models. The DEGs from RNA-seq analyses were compared between patients with PH and donor controls, and between DAHP or hypoxia-induced PH mice and control mice. $P<0.05$ was considered significant. A total number of 4548, 733, and 439 DEGs were identified by RNA-seq analyses in patients with pulmonary arterial hypertension (PAH) (PAH, n=12 vs controls, n=10), DAHP-treated mice (n=3 each), and hypoxia-treated mice (n=3 each), respectively. Note that the overlap of DEGs between human PH and hypoxia model is 123, whereas the overlap between human PH and DAHP model is 325, indicating that the DAHP model displayed more similar gene regulatory profiles as in patients with human PH.

DISCUSSION

The most significant advancements of the current study are (1) establishment of a novel murine model of PH that simulates human disease; (2) demonstration of a novel therapeutic role of endothelial-specific targeting of DHFR for PH, along with definition of an intrinsic role of DHFR deficiency in causing PH; and (3) demonstration of a robust effect of DHFR overexpression on the complete regression of PH in both novel and classical models of PH. By targeting the endothelium directly with DAHP administration to induce uncoupling of eNOS, we found that DAHP-treated mice developed time-dependent increases in mPAP and RVSP, and a full spectrum of vascular lesions that simulate human disease. The animals also displayed phenotypes of increased total superoxide and mitochondrial superoxide production and uncoupling of eNOS with reduced NO and tetrahydrobiopterin bioavailabilities. More intriguingly, we demonstrated that endothelial-specific DHFR transgenic mice (tg-EC-DHFR) were completely protected from PH development in both DAHP and hypoxia-induced models of PH, as evidenced by abrogated mPAP and RVSP, attenuated ROS production, preserved NO bioavailability, restored eNOS coupling activity, and ultimately diminished vascular remodeling and formation of a full spectrum of vascular lesions compared with the DAHP- or hypoxia-treated WT mice. DHFR knockout mice, by contrast, exhibited obvious PH phenotypes as in DAHP or hypoxia models, demonstrating an intrinsic role of DHFR deficiency in causing PH. In addition, DHFR knockout mice exposed to hypoxia exhibited similar phenotypes as DHFR KO mice, which indicates no additional effects of hypoxia further validating an intermediate role of DHFR deficiency in PH development. In addition, overexpression of DHFR after initiation of PH with pCMV-DHFR plasmid transfection revealed robust reversal effects on PH phenotypes, including improved hemodynamics, attenuated ROS production, preserved NO and tetrahydrobiopterin bioavailabilities, restored eNOS coupling activity, and complete abrogation of pulmonary vascular remodeling including formation of all of the vascular lesions in both DAHP and hypoxia models. Importantly, RNA-seq analyses of lung samples from patients with human PH and DAHP and hypoxic models indicated greater similarity in

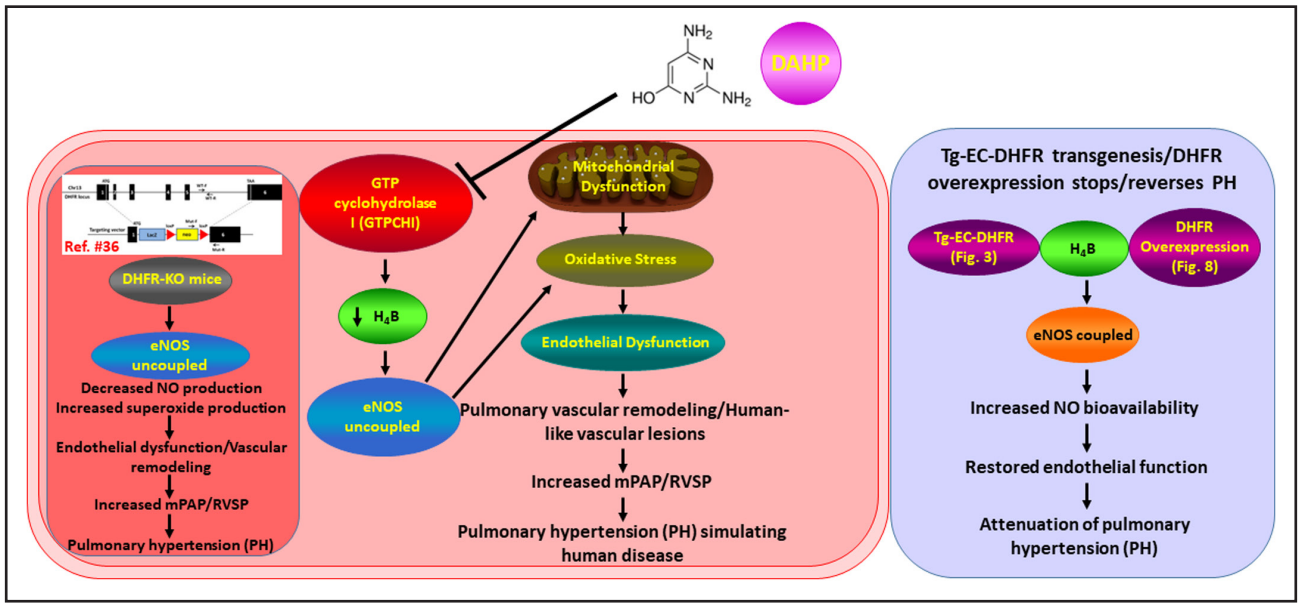

Figure 10. A novel murine model of pulmonary hypertension (PH) that simulates human disease of PH and endothelial-specific targeting of dihydrofolate reductase (DHFR) as a novel and robust therapy for PH.
DAHP (2,4-diamino 6-hydroxypyrimidine) induces inhibition of GTP cyclohydrolase 1 (GTPCHI) and eNOS (endothelial nitric oxide synthase) uncoupling activity, resulting in mitochondrial dysfunction, persistent oxidative stress, and endothelial dysfunction. This leads to the development of PH that is human-like in pathophysiological features characterized by a full spectrum of vascular lesions as observed in patients with human PH. DAHP induces significant elevations in mean pulmonary arterial pressure (mPAP) and right ventricular systolic blood pressure (RVSP), extensive vascular remodeling, nitric oxide (NO) deficiency, increased total and mitochondrial superoxide production, and the formation of typical human-like vascular lesions in the lung. Endothelial-specific DHFR transgenesis in tg-EC-DHFR mice is robustly effective in abolishing all pathophysiological phenotypes and molecular changes of PH induced by DAHP or hypoxia exposure. DHFR knockout (KO) mice display PH phenotypes at baseline that is comparable to DAHP and hypoxia models, and there is no additional effect with hypoxia exposure, indicating an intrinsic role of DHFR deficiency in mediating the development of PH. Therefore, targeting DHFR specifically in the endothelium proves to be an innovative and robust therapeutic strategy for PH. H_4B indicates tetrahydrobiopterin; and WT, wild type.

gene regulation profiles between the DAHP-induced PH model (versus the hypoxia-induced model of PH) and human patients with PH. Thus, our data not only establish a novel human-like murine model of PH that can be used broadly for mechanistic and translational studies but also demonstrate a novel and robust therapeutic potential of targeting endothelial DHFR for the treatment and reversal of PH. These findings and concepts are graphically illustrated in Figure 10.

The search for better preclinical models of PH continues; and yet, to date, with no success in establishing a single model has all of the features of human disease.[1,50] Evidence suggests that medial hypertrophy, which is the most consistent pathological finding in idiopathic PH due to enhanced vascular smooth muscle cell proliferation, can result in lumen obliteration.[51] DAHP administration induced medial thickness, particularly in the smaller vessels (<200 μm), in contrast to the predominance of nonmuscular arterioles in the control group. Several studies and reviews conclude that the pathological lesions in Sugen5416/hypoxia rats are indistinguishable from those in human PH (summarized in reference [52]); however, recent reports directly assessing the pathology conclude that even the SU5416-hypoxia model lesions do not compare with the recanalized plexogenic lesions in humans.[18] In addition, plexiform lesions were reported to develop via pulmonary microvascular EC proliferation in humans and rats. To determine whether a similar process occurs in DAHP-treated mice, we compared histopathologic features and found similar plexiform lesions and recanalized vascular lesions compared with that of the human disease. Our results indicate that 9 weeks of treatment with DAHP resulted in medial thickening, intimal thickness, formation of plexiform lesions, aneurysm-like lesions, anarchous growth of cells that completely obliterate the vascular lumen, bud-like lesions covered by an endothelial layer, disorganized stalk-like lesions comprising hyperchromatic and oval cells inside the lumen of pulmonary arteries, and recanalized lesions. For histological analyses, the middle lobe of the left lung of all experimental groups was consistently fixed in 4% paraformaldehyde overnight, embedded, and subjected to H&E. The plexiform lesion is a characteristic structure of the pulmonary arteriopathy of severe PH. Our data indicate upregulation of SMA in the lung tissue sections of DAHP-induced PH mice. Of note, DAHP is an effective stimulus for pulmonary arterial smooth muscle cell (PASMC) proliferation as demonstrated by markedly upregulated PCNA expression, consequent to eNOS uncoupling, and a loss in NO bioavailability. Proliferative

arrest induced by endogenous NO production has been found in different cell types, including vascular smooth muscle cells (VSMCs).[53] Preclinical models have been essentially used to establish the potential of NO in the inhibition of VSMC proliferation in models of neointimal hyperplasia and restenosis.[54] Collagen accumulation and deposition increase pulmonary arterial stiffening, which facilitates the progression of PH and, eventually, RV dysfunction.[10] In this study, we observed a significant increase in collagen deposition in the perivascular and peribronchial areas of the pulmonary arteries of DAHP-treated mice.

Because the data from the novel DAHP model have demonstrated a critical direct causal role of eNOS uncoupling in the development of PH, we studied potential therapeutic effects of endothelial-specific overexpression of DHFR using a novel in-house generated mouse strain of tg-EC-DHFR. We have previously established that endothelial DHFR deficiency is a major mediator of eNOS uncoupling and eNOS uncoupling-driven pathogenesis of vascular diseases, including hypertension, aortic aneurysms, and diabetic vascular dysfunction.[21–41] Indeed, our data demonstrated that tg-EC-DHFR mice were completely protected from developing PH in response to both DAHP and hypoxia stimulation. The hemodynamic changes of increased mPAP and RVSP in response to DAHP treatment or hypoxia exposure were completely abrogated, indicating that tg-EC-DHFR mice are unresponsive to DAHP or hypoxia-induced pulmonary vasoconstriction and progressive RV hypertrophy. In tg-EC-DHFR mice, the wall thickening was decreased in the media of small-sized pulmonary arteries, which was accompanied by reduced expression of SMA and PCNA. DAHP or hypoxia-induced pulmonary collagen deposition was also attenuated in tg-EC-DHFR mice. Fluorescent imaging with DAF-FM DA, DHE, and MitoSOX revealed restored NO bioavailability and attenuated total and mitochondrial superoxide production. Electron spin resonance data indicated restored eNOS coupling activity, while HPLC data showed increased tetrahydrobiopterin bioavailability in tg-EC-DHFR mice despite DAHP or hypoxia exposure. Therefore, recoupling of eNOS in tg-EC-DHFR mice completely protected against development of PH in DAHP or hypoxia-treated mice at pathophysiological and molecular levels, indicating a novel therapeutic option of targeting endothelial DHFR deficiency for the treatment of PH.

More importantly, overexpression of DHFR after initiation of PH resulted in a remarkable reversal of PH phenotypes in DAHP- or hypoxia-treated mice. Mice transfected with pCMV-DHFR plasmid following initiation of PH by DAHP or hypoxia exposure manifested complete reversal of PH phenotypes at pathophysiological and molecular levels as described above in tg-EC-DHFR mice. Consistent with the above findings, our data provide ample evidence from several analyses that DHFR overexpression reversed PH as evidenced by improved hemodynamics, restored NO and tetrahydrobiopterin bioavailabilities, attenuated total and mitochondrial superoxide production, and abrogated eNOS uncoupling activity, as well as diminished vascular remodeling and formation of vascular lesions. Thus, targeting endothelial DHFR is effective in preventing, treating, and reversing PH in both novel and classical murine models of DAHP- and hypoxia-induced PH, respectively. In addition, this strategy might have broad applicability to other genetic or nongenetic models of PH or to patients with PH of different types derived from different original diseases/pathological conditions.

We have recently generated a novel strain of DHFR knockout mice[36,37] and used it in the current study to examine a potential intrinsic role of DHFR deficiency in causing PH. Intriguingly, DHFR knockout mice displayed robust PH phenotypes at baseline. We observed increased mPAP and RVSP, medial thickening, upregulation of SMA and PCNA, increased collagen deposition, reduced NO bioavailability, increased total and mitochondrial superoxide production, and eNOS uncoupling activity in DHFR knockout mice. These data seem to share some similarities with our previous findings that an endothelial-specific deficiency in DHFR underlies development of systematic disorders of hypertension and aortic aneurysms in Ang II infused WT mice, hph-1 mice, and apoE null mice.[21,23,24,32,34–41] This observation also further aligns with the robust therapeutic effect of endothelial-specific DHFR transgenesis in protecting against PH in the tg-EC-DHFR mice. Of note, hypoxia treatment of the DHFR knockout mice showed no additional worsening in PH phenotypes, indicating an intrinsic role of DHFR deficiency in mediating hypoxia-induced PH.

To compare similarities in gene regulation profiles between the new DAHP model (versus the hypoxia model) and human PH, we performed RNA-seq analyses on lung samples isolated from DAHP and hypoxia mice, and on explanted lung samples collected from donor controls and PH patients undergoing transplantation surgery. The significantly regulated genes (DEGs) from the RNA-seq analyses were compared between patients with PH and healthy donors or between mouse models and control groups. The overlap of DEGs between human PH and the hypoxia model is 123 (DEGs), whereas the overlap between human PH and the DAHP model is 325 (DEGs), suggesting that the DAHP model has much more similarity to human PH at the level of gene regulation, in contrast to the hypoxia model. Recent studies on RNA-seq-based expression profiles identified *ZNF841*, *CLASP2*, and *CSNK1E* as some of the top genes involved in hyperproliferative cellular processes, which is highly relevant to vascular remodeling observed in PAH.[55] Our study is the first to compare gene expression analyses between DAHP-induced PH and human PH, and these data provide evidence of additional characteristic features of the human-like model of PH induced by DAHP.

CONCLUSIONS

In conclusion, the present study for the first time establishes a novel murine model of PH that simulates human PH, and a novel and robust effect of targeting endothelial DHFR deficiency for the treatment and reversal of PH. DAHP induces uncoupling of eNOS, subsequent superoxide production and NO deficiency, and extensive vascular remodeling and formation of typical human-like vascular lesions in the lung, with development and progression of PH characterized by increases in mPAP, RVSP, and RV/(LV+S) ratio. Endothelial DHFR transgenesis is robustly effective in abolishing all elements of the PH phenotype. DHFR knockout in mice, however, leads to PH phenotypes comparable to DAHP or hypoxia model and shows no additional features when treated with hypoxia, indicating an intrinsic role of DHFR deficiency in causing PH. The novel human-like DAHP model of PH would, no doubt, enable further mechanistic and translational studies, while endothelial specific targeting of DHFR deficiency represents an innovative and robust therapeutic strategy for PH.

ARTICLE INFORMATION

Received May 15, 2023; revision received January 6, 2024; accepted January 15, 2024.

Affiliations

Division of Molecular Medicine, Department of Anesthesiology, Division of Cardiology, Department of Medicine, David Geffen School of Medicine, University of California, Los Angeles (P.M., Y.Z., Y.H., N.C.Z., J.Y.Y., H.C.). Peking Union Medical College and Chinese Academy of Medical Sciences, Department of Respiratory Medicine, China-Japan Friendship Hospital, Beijing (W.C., C.W.). Department of Medicine, Brigham and Women's Hospital, Harvard Medical School, Boston, MA (J.L.).

Sources of Funding

This work was supported by the National Heart, Lung, and Blood Institute grants HL077440 (to H. Cai), HL088975 (to H. Cai), HL142951 (to H. Cai), HL154754 (to H. Cai and A.M.), HL162407 (to H. Cai and J.G.), HL142951-03S1 (to H. Cai), and HL154754-03S1 (to H. Cai).

Disclosures

None.

Supplemental Material

Expanded Materials and Methods
References 56–62
Major Resources Table
ARRIVE Guidelines

REFERENCES

1. Chan SY, Loscalzo J. Pulmonary vascular disease related to hemodynamic stress in the pulmonary circulation. *Compr Physiol.* 2011;1:123–139. doi: 10.1002/cphy.c090004
2. Vonk Noordegraaf A, Chin KM, Haddad F, Hassoun PM, Hemnes AR, Hopkins SR, Kawut SM, Langleben D, Lumens J, Naeije R. Pathophysiology of the right ventricle and of the pulmonary circulation in pulmonary hypertension: an update. *Eur Respir J.* 2019;53:1801900. doi: 10.1183/13993003.01900-2018
3. Raiesdana A, Loscalzo J. Pulmonary arterial hypertension. *Ann Med.* 2006;38:95–110. doi: 10.1080/07853890600622143
4. Morrell NW, Adnot S, Archer SL, Dupuis J, Lloyd Jones P, MacLean MR, McMurtry IF, Stenmark KR, Thistlethwaite PA, Weissmann N, et al. Cellular and molecular basis of pulmonary arterial hypertension. *J Am Coll Cardiol.* 2009;54:S20–S31. doi: 10.1016/j.jacc.2009.04.018
5. Farber HW, Loscalzo J. Prothrombotic mechanisms in primary pulmonary hypertension. *J Lab Clin Med.* 1999;134:561–566. doi: 10.1016/s0022-2143(99)90094-x
6. Loscalzo J. Endothelial dysfunction in pulmonary hypertension. *N Engl J Med.* 1992;327:117–119. doi: 10.1056/NEJM199207093270209
7. Voelkel NF, Cool C, Taraceviene-Stewart L, Geraci MW, Yeager M, Bull T, Kasper M, Tuder RM. Janus face of vascular endothelial growth factor: the obligatory survival factor for lung vascular endothelium controls precapillary artery remodeling in severe pulmonary hypertension. *Crit Care Med.* 2002;30:S251–S256. doi: 10.1097/00003246-200205001-00013
8. Loh E, Stamler JS, Hare JM, Loscalzo J, Colucci WS. Cardiovascular effects of inhaled nitric oxide in patients with left ventricular dysfunction. *Circulation.* 1994;90:2780–2785. doi: 10.1161/01.cir.90.6.2780
9. Napoli C, Loscalzo J. Nitric oxide and other novel therapies for pulmonary hypertension. *J Cardiovasc Pharmacol Ther.* 2004;9:1–8. doi: 10.1177/107424840400900i101
10. Maron BA, Goldstein RH, Rounds SI, Shapiro S, Jankowich M, Garshick E, Moy ML, Gagnon D, Choudhary G. Study design and rationale for investigating phosphodiesterase type 5 inhibition for the treatment of pulmonary hypertension due to chronic obstructive lung disease: the TADA-PHiLD (TADAlafil for Pulmonary Hypertension associated with chronic obstructive Lung Disease) trial. *Pulm Circ.* 2013;3:889–897. doi: 10.1086/674759
11. Woodcock CC, Chan SY. The search for disease-modifying therapies in pulmonary hypertension. *J Cardiovasc Pharmacol Ther.* 2019;24:334–354. doi: 10.1177/1074248419829172
12. Stenmark KR, Meyrick B, Galie N, Mooi WJ, McMurtry IF. Animal models of pulmonary arterial hypertension: the hope for etiological discovery and pharmacological cure. *Am J Physiol Lung Cell Mol Physiol.* 2009;297:L1013–L1032. doi: 10.1152/ajplung.00217.2009
13. Song Y, Jones JE, Beppu H, Keaney JF Jr, Loscalzo J, Zhang YY. Increased susceptibility to pulmonary hypertension in heterozygous BMPR2-mutant mice. *Circulation.* 2005;112:553–562. doi: 10.1161/CIRCULATIONAHA.104.492488
14. Maarman G, Lecour S, Butrous G, Thienemann F, Sliwa K. A comprehensive review: the evolution of animal models in pulmonary hypertension research; are we there yet? *Pulm Circ.* 2013;3:739–756. doi: 10.1086/674770
15. Murugesan P, Hildebrandt T, Bernlöhr C, Lee D, Khang G, Doods H, Wu D. Inhibition of kinin B1 receptors attenuates pulmonary hypertension and vascular remodeling. *Hypertension.* 2015;66:906–912. doi: 10.1161/HYPERTENSIONAHA.115.05338
16. Hill NS, Gillespie MN, McMurtry IF. Fifty years of monocrotaline-induced pulmonary hypertension: what has it meant to the field? *Chest.* 2017;152:1106–1108. doi: 10.1016/j.chest.2017.10.007
17. Nicolls MR, Mizuno S, Taraseviciene-Stewart L, Farkas L, Drake JI, Al Husseini A, Gomez-Arroyo JG, Voelkel NF, Bogaard HJ. New models of pulmonary hypertension based on VEGF receptor blockade-induced endothelial cell apoptosis. *Pulm Circ.* 2012;2:434–442. doi: 10.4103/2045-8932.105031
18. Vitali SH, Hansmann G, Rose C, Fernandez-Gonzalez A, Scheid A, Mitsialis SA, Kourembanas S. The Sugen 5416/hypoxia mouse model of pulmonary hypertension revisited: long-term follow-up. *Pulm Circ.* 2014;4:619–629. doi: 10.1086/678508
19. Ciuclan L, Bonneau O, Hussey M, Duggan N, Holmes AM, Good R, Stringer R, Jones P, Morrell NW, Jarai G, et al. A novel murine model of severe pulmonary arterial hypertension. *Am J Respir Crit Care Med.* 2011;184:1171–1182. doi: 10.1164/rccm.201103-0412OC
20. Gomez-Arroyo J, Saleem SJ, Mizuno S, Syed AA, Bogaard HJ, Abbate A, Taraseviciene-Stewart L, Sung Y, Kraskauskas D, Farkas D, et al. A brief overview of mouse models of pulmonary arterial hypertension: problems and prospects. *Am J Physiol Lung Cell Mol Physiol.* 2012;302:L977–L991. doi: 10.1152/ajplung.00362.2011
21. Chalupsky K, Cai H. Endothelial dihydrofolate reductase: critical for nitric oxide bioavailability and role in angiotensin II uncoupling of endothelial nitric oxide synthase. *Proc Natl Acad Sci U S A.* 2005;102:9056–9061. doi: 10.1073/pnas.0409594102
22. Oak JH, Cai H. Attenuation of angiotensin II signaling recouples eNOS and inhibits nonendothelial NOX activity in diabetic mice. *Diabetes.* 2007;56:118–126. doi: 10.2337/db06-0288
23. Gao L, Chalupsky K, Stefani E, Cai H. Mechanistic insights into folic acid-dependent vascular protection: dihydrofolate reductase (DHFR)-mediated reduction in oxidant stress in endothelial cells and angiotensin II-infused

mice. A novel HPLC-based fluorescent assay for DHFR activity. *J Mol Cell Cardiol*. 2009;47:752–760. doi: 10.1016/j.yjmcc.2009.07.025
24. Gao L, Siu KL, Chalupsky K, Nguyen A, Chen P, Weintraub NL, Galis Z, Cai H. Role of uncoupled endothelial nitric oxide synthase in abdominal aortic aneurysm formation: treatment with folic acid. *Hypertension*. 2012;59:158–166. doi: 10.1161/HYPERTENSIONAHA.111.181644
25. Zhang J, Cai H. Netrin-1 prevents ischemia/reperfusion-induced myocardial infarction via a DCC/ERK1/2/eNOS(s1177)/NO/DCC feed-forward mechanism. *J Mol Cell Cardiol*. 2010;48:1060–1070. doi: 10.1016/j.yjmcc.2009.11.020
26. Youn JY, Gao L, Cai H. The p47phox- and NADPH oxidase organiser 1 (NOXO1)-dependent activation of NADPH oxidase 1 (NOX1) mediates endothelial nitric oxide synthase (eNOS) uncoupling and endothelial dysfunction in a streptozotocin-induced murine model of diabetes. *Diabetologia*. 2012;55:2069–2079. doi: 10.1007/s00125-012-2557-6
27. Siu KL, Miao XN, Cai H. Recoupling of eNOS with folic acid prevents abdominal aortic aneurysm formation in angiotensin II-infused apolipoprotein E null mice. *PLoS One*. 2014;9:e88899. doi: 10.1371/journal.pone.0088899
28. Bouhidel JO, Wang P, Li Q, Cai H. Pharmacological postconditioning treatment of myocardial infarction with netrin-1. *Front Biosci (Landmark Ed)*. 2014;19:566–570. doi: 10.2741/4227
29. Bouhidel JO, Wang P, Siu KL, Li H, Youn JY, Cai H. Netrin-1 improves post-injury cardiac function in vivo via DCC/NO-dependent preservation of mitochondrial integrity, while attenuating autophagy. *Biochim Biophys Acta*. 2015;1852:277–289. doi: 10.1016/j.bbadis.2014.06.005
30. Li Q, Wang P, Ye K, Cai H. Central role of SIAH inhibition in DCC-dependent cardioprotection provoked by netrin-1/NO. *Proc Natl Acad Sci U S A*. 2015;112:899–904. doi: 10.1073/pnas.1420695112
31. Li Q, Cai H. Induction of cardioprotection by small netrin-1-derived peptides. *Am J Physiol Cell Physiol*. 2015;309:C100–C106. doi: 10.1152/ajpcell.00332.2014
32. Miao XN, Siu KL, Cai H. Nifedipine attenuation of abdominal aortic aneurysm in hypertensive and non-hypertensive mice: Mechanisms and implications. *J Mol Cell Cardiol*. 2015;87:152–159. doi: 10.1016/j.yjmcc.2015.07.031
33. Li Q, Youn JY, Cai H. Mechanisms and consequences of endothelial nitric oxide synthase dysfunction in hypertension. *J Hypertens*. 2015;33:1128–1136. doi: 10.1097/HJH.0000000000000587
34. Siu KL, Li Q, Zhang Y, Guo J, Youn JY, Du J, Cai H. NOX isoforms in the development of abdominal aortic aneurysm. *Redox Biol*. 2017;11:118–125. doi: 10.1016/j.redox.2016.11.002
35. Li H, Li Q, Zhang Y, Liu W, Gu B, Narumi T, Siu KL, Youn JY, Liu P, Yang X, et al. Novel treatment of hypertension by specifically targeting E2F for restoration of endothelial dihydrofolate reductase and eNOS function under oxidative stress. *Hypertension*. 2019;73:179–189. doi: 10.1161/HYPERTENSIONAHA.118.11643
36. Li Q, Youn JY, Siu KL, Murugesan P, Zhang Y, Cai H. Knockout of dihydrofolate reductase in mice induces hypertension and abdominal aortic aneurysm via mitochondrial dysfunction. *Redox Biol*. 2019;24:101185. doi: 10.1016/j.redox.2019.101185
37. Zhang Y, Murugesan P, Huang K, Cai H. NADPH oxidases and oxidase crosstalk in cardiovascular diseases: novel therapeutic targets. *Nat Rev Cardiol*. 2020;17:170–194. doi: 10.1038/s41569-019-0260-8
38. Huang K, Narumi T, Zhang Y, Li Q, Murugesan P, Wu Y, Liu NM, Cai H. Targeting MicroRNA-192-5p, a downstream effector of NOXs (NADPH Oxidases), reverses endothelial DHFR (Dihydrofolate Reductase) deficiency to attenuate abdominal aortic aneurysm formation. *Hypertension*. 2021;78:282–293. doi: 10.1161/HYPERTENSIONAHA.120.15070
39. Huang K, Wang Y, Siu KL, Zhang Y, Cai H. Targeting feed-forward signaling of TGFβ/NOX4/DHFR/eNOS uncoupling/TGFβ axis with anti-TGFβ and folic acid attenuates formation of aortic aneurysms: novel mechanisms and therapeutics. *Redox Biol*. 2021;38:101757. doi: 10.1016/j.redox.2020.101757
40. Huang K, Wu Y, Zhang Y, Youn JY, Cai H. Combination of folic acid with nifedipine is completely effective in attenuating aortic aneurysm formation as a novel oral medication. *Redox Biol*. 2022;58:102521. doi: 10.1016/j.redox.2022.102521
41. Zhang Y, Siu KL, Li Q, Howard-Quijano K, Scovotti J, Mahajan A, Cai H. Diagnostic and predictive values of circulating tetrahydrobiopterin levels as a novel biomarker in patients with thoracic and abdominal aortic aneurysms. *Redox Biol*. 2022;56:102444. doi: 10.1016/j.redox.2022.102444
42. Gross SS, Levi R. Tetrahydrobiopterin synthesis. an absolute requirement for cytokine-induced nitric oxide generation by vascular smooth muscle. *J Biol Chem*. 1992;267:25722–25729.
43. Ozaki M, Kawashima S, Yamashita T, Ohashi Y, Rikitake Y, Inoue N, Hirata KI, Hayashi Y, Itoh H, Yokoyama M. Reduced hypoxic pulmonary vascular remodeling by nitric oxide from the endothelium. *Hypertension*. 2001;37:322–327. doi: 10.1161/01.hyp.37.2.322
44. Chalupsky K, Kračun D, Kanchev I, Bertram K, Görlach A. Folic acid promotes recycling of tetrahydrobiopterin and protects against hypoxia-induced pulmonary hypertension by recoupling endothelial nitric oxide synthase. *Antioxid Redox Signal*. 2015;23:1076–1091. doi: 10.1089/ars.2015.6329
45. Budhiraja R, Tuder RM, Hassoun PM. Endothelial dysfunction in pulmonary hypertension. *Circulation*. 2004;109:159–165. doi: 10.1161/01.CIR.0000102381.57477.50
46. Wilkins MR. Pulmonary hypertension: the science behind the disease spectrum. *Eur Respir Rev*. 2012;21:19–26. doi: 10.1183/09059180.00008411
47. Condon DF, Nickel NP, Anderson R, Mirza S, de Jesus Perez VA. The 6th World Symposium on Pulmonary Hypertension: what's old is new. *F1000Res*. 2019;8:F1000 Faculty Rev. doi: 10.12688/f1000research.18811.1
48. Abe K, Toba M, Alzoubi A, Ito M, Fagan KA, Cool CD, Voelkel NF, McMurtry IF, Oka M. Formation of plexiform lesions in experimental severe pulmonary arterial hypertension. *Circulation*. 2010;121:2747–2754. doi: 10.1161/CIRCULATIONAHA.109.927681
49. Sutendra G, Michelakis ED. Pulmonary arterial hypertension: challenges in translational research and a vision for change. *Sci Transl Med*. 2013;5:208sr–20205. doi: 10.1126/scitranslmed.3005428
50. Hong KH, Lee YJ, Lee E, Park SO, Han C, Beppu H, Li E, Raizada MK, Bloch KD, Oh SP. Genetic ablation of the BMPR2 gene in pulmonary endothelium is sufficient to predispose to pulmonary arterial hypertension. *Circulation*. 2008;118:722–730. doi: 10.1161/CIRCULATIONAHA.107.736801
51. Mandegar M, Fung YC, Huang W, Remillard CV, Rubin LJ, Yuan JX. Cellular and molecular mechanisms of pulmonary vascular remodeling: role in the development of pulmonary hypertension. *Microvasc Res*. 2004;68:75–103. doi: 10.1016/j.mvr.2004.06.001
52. Taichman DB, Mandel J. Epidemiology of pulmonary arterial hypertension. *Clin Chest Med*. 2013;34:619–637. doi: 10.1016/j.ccm.2013.08.010
53. Villalobo A. Nitric oxide and cell proliferation. *FEBS J*. 2006;273:2329–2344. doi: 10.1111/j.1742-4658.2006.05250.x
54. Hogg ME, Varu VN, Vavra AK, Popowich DA, Banerjee MN, Martinez J, Jiang Q, Saavedra JE, Keefer LK, Kibbe MR. Effect of nitric oxide on neointimal hyperplasia based on sex and hormone status. *Free Radic Biol Med*. 2011;50:1065–1074. doi: 10.1016/j.freeradbiomed.2011.01.016
55. Romanoski CE, Qi X, Sangam S, Vanderpool RR, Stearman RS, Conklin A, Gonzalez-Garay M, Rischard F, Ayon RJ, Wang J, et al. Transcriptomic profiles in pulmonary arterial hypertension associate with disease severity and identify novel candidate genes. *Pulm Circ*. 2020;10:2045894020968531. doi: 10.1177/2045894020968531
56. Bombicz M, Priksz D, Varga B, Kurucz A, Kertész A, Takacs A, Posa A, Kiss R, Szilvassy Z, Juhasz B. A Novel therapeutic approach in the treatment of pulmonary arterial hypertension: allium ursinum liophylisate alleviates symptoms comparably to sildenafil. *Int J Mol Sci*. 2017;18:1436. doi: 10.3390/ijms18071436
57. Pan M, Han Y, Si R, Guo R, Desai A, Makino A. Hypoxia-induced pulmonary hypertension in type 2 diabetic mice. *Pulm Circ*. 2017;7:175–185. doi: 10.1086/690206
58. Li C, Xu D, Ye Q, Hong S, Jiang Y, Liu X, Zhang N, Shi L, Qin CF, Xu Z. Zika virus disrupts neural progenitor development and leads to microcephaly in mice. *Cell Stem Cell*. 2016;19:120–126. doi: 10.1016/j.stem.2016.04.017
59. Su H, Hu J, Huang L, Yang Y, Thenoz M, Kuchmiy A, Hu Y, Li P, Feng H, Zhou Y, et al. SHQ1 regulation of RNA splicing is required for T-lymphoblastic leukemia cell survival. *Nat Commun*. 2018;9:4281. doi: 10.1038/s41467-018-06523-4
60. Langmead B, Salzberg SL. Fast gapped-read alignment with Bowtie 2. *Nat Methods*. 2012;9:357–359. doi: 10.1038/nmeth.1923
61. Li B, Dewey CN. RSEM: accurate transcript quantification from RNA-Seq data with or without a reference genome. *BMC Bioinf*. 2011;12:323. doi: 10.1186/1471-2105-12-323
62. Robinson MD, McCarthy DJ, Smyth GK. edgeR: a Bioconductor package for differential expression analysis of digital gene expression data. *Bioinformatics*. 2010;26:139–140. doi: 10.1093/bioinformatics/btp616